The behavior of vertically non-homogeneous elastic solids under internal rectangular loads

Yunyue Xie[1,2], Hongtian Xiao[*1], Zhongqi Quentin Yue[3]

1. College of Civil Engineering & Architecture, Shandong Univ. of Sci. & Tech., Qingdao, P. R. China.
2. State Key Laboratory of Mining Disaster Prevention and Control Cofounded by Shandong Province and the MOST of China, Qingdao, P. R. China.
3. Department of Civil Engineering, The University of Hong Kong, Hong Kong, P. R. China.

Abstract: This paper examines the internal rectangular loading problems for an elastic halfspace where the shear modulus varies exponentially or linearly and the Poisson's ratio keeps constant or varies linearly with depth. The numerical method is developed through applying the fundamental solution of layered elastic solids and integrating numerically it over the loading area. The adaptive integration of the displacement and traction integrals over the loading area is designed to calculate the nearly singular integral for the source point close to an element. The discretization approach is applied to deal with an arbitrarily depth-heterogeneous elastic solid. OpenMP directives are used to parallelize the internal loop, which controls element iterations so that a high computing speed can be obtained. For an axisymmetric internal loading problem, the displacements obtained with the present formulation are in very good agreement with existing closed-form solutions. Finally, stresses and displacements in non-homogeneous halfspaces induced by horizontally and vertically uniform rectangular loadings are presented. Results illustrate the effect of non-homogeneous properties on the stress and displacement fields.

Key words: non-homogeneous elastic solids, rectangular loading area, numerical modeling, adaptive numerical integration, parallelized computation, displacements and stresses

[*]Corresponding Author. Tel: +86-532-80681200.

E-mail addresses: xiaohongtian@tsinghua.org.cn (H. T. Xiao).

1. Introduction

1.1 Background

Intact soils and rocks exhibit strong spatial variations in the material properties because of their natural formation process (Zhao et al., 2016; Guo & Zhao, 2016). In some cases, materials has their physical and mechanical properties variable along a given coordinate and keeping constant along the other two coordinates perpendicular to the given coordinate. For example, the geotechnical investigations to soils showed that the shear modulus of undrained soils varied linearly with depth (Abbiss, 1979). It has been well recognized that non-homogeneity of materials has a significant effect on the stresses and deformations in the material region under loadings. The elastic responses of non-homogeneous solids subjected to loadings have been of great interest to many researchers and engineers in applied mechanics and many branches of engineering (Selvadurai, 2007).

The problems related to the mechanics of non-homogeneous geo-materials are much difficult to be solved and can be simplified via the following assumptions. The first is to model the geo-material as a homogeneous or piece-wisely homogeneous elastic solid in engineering analysis (Chen, 1971; Pan, 1989; Yue, Yin & Zhang, 1999; Pan et al., 2007; Zhang, Liu & Lin, 2016; Zhang et al. 2016). The second is to assume that the shear modulus of a non-homogeneous medium varies continuously with depth. Some of the earliest researchers (Rostovtsev, 1964) used a power law function for considering the variations of shear modulus with depth. As a special case of the power law function, the linear variation of shear modulus with depth was widely applied by Gibson (1967). The exponential variation of shear modulus with depth has also been assumed for analysis of non-homogeneous geo-materials under different types of loads by Selvadurai et al. (1986), Rajapakse et al. (1989), Stark et al. (1997), etc. For easy analysis, it is usually assumed that the Poisson's ratio of the nonhomogeneous solids keeps constant and does not vary with depth.

The displacements and stresses resulting from a footing load are important parameters in the design of foundations. This kind of loads uniformly distributed on the horizontal surface plays a predominant role for engineering design, and the distributed rectangular loading can be considered as a realistic loading situation. The numerical solutions of such loading can have direct applications to many problems encountered in geo-mechanics and engineering. Marmo et al. (2016) and Marmo & Rosati (2016) developed the analytical solutions of elastic fields within an homogeneous isotropic halfspace subject to linearly varying horizontal loads distributed on polygonal regions of its surface. Marmo et al. (2017) further presented analytical expressions of

transversely isotropic halfspaces subject to linearly distributed vertical pressures applied over arbitrary regions of the halfspace boundary. However, it is much difficult to obtain the solution of the analytical solutions of the non-homogeneous halfspaces subjected to complex loadings. It should be pointed out that Booker et al. (1985) developed a numerical procedure to determine the surface displacements of a non-homogeneous soil subjected to various surface loads, such as point and line loads or uniformly distributed tractions. Furthermore, Doherty et al. (2003) developed the scaled boundary finite-element method for analysis of a non-homogeneous elastic halfspace subjected to a variety of surface loadings. In the above analyses, a power-law function is used to describe the variation of elastic modulus with depth. More recently, Katebi & Selvadurai (2013) and Selvadurai & Katebi (2013) analyzed the axisymmetric problem of the internal loading of incompressible halfspaces with an exponential variation with depth. Actually, depth-dependent non-homogeneity is distributed in a much complex form and an effective analyzing approach should model arbitrary variations with depth.

1.2 Aim and approach of this study

The objective of this paper is to present numerical solutions for a non-homogeneous half-space subjected to internal loadings in both vertical and horizontal directions, as shown in Fig. 1. The loadings are uniformly distributed on a rectangular area. The rectangular loading area is horizontally parallel to the boundary surface. To the authors' best knowledge, the numerical solutions for this elastic problem are not available in the relevant literature. The geo-materials to be studied can have their elastic properties exhibiting arbitrary variations in depth and keeping constant in lateral directions.

The numerical method to be utilized is based on the fundamental solutions for a multilayered elastic solids of infinite extent subjected to concentrated body force vectors developed by Yue (1995). Using this fundamental solution, Xiao, Yue, & Zhao (2012) developed the numerical methods for analyzing elastic fields in heterogeneous rocks due to reservoir water impoundment. This paper further develops this numerical method to obtain highly accurate solutions of a non-homogeneous solid subjected to different types of distributed loads. The proposed method utilizes the integral method on the loading area and discretizes the loading area by four- or eight-noded elements. The integral on every element is executed using effective numerical methods. The proposed numerical method is characterized by a parallel nature. A straight approach is to use OpenMP directives to parallelize the loop for element iterations. It is known that the elastic fields vary sharply as the field point has a very small distance to a loading area. In this paper, an improved numerical method will be developed to obtain a highly accurate solution. Specially, the

variations of the Poisson's ratio with depth are considered. Results show the influence of the non-homogeneity on the displacements and stresses of a non-homogeneous elastic halfspace under uniform internal loading over a rectangular area.

2. The numerical method of analyzing a non-homogeneous halfspace

2.1 Fundamental solutions of multi-layered solids subject to concentrated point loads

The fundamental solution is the analytical solution for the elastostatic field in a layered solid of infinite extent due to the action of concentrated point loads. The dissimilar homogeneous layers adhere an elastic solid of upper semi-infinite extent and another elastic solid of lower semi-infinite extent. The interface between any two connected dissimilar layers is fully bonded. It was given by Yue (1995) and also called as Yue's solution (Maloney et al., 2008; Buxboim et al., 2010; Merkel et al., 2007).

The results illustrated that numerical evaluation of the solution can be achieved with controlled accuracy. The solution is characterized by an elastic solid with any layers and high efficiency. The convergence of the solution has been verified and the solution satisfies all the required conditions including the basic equations and the interfacial conditions as well as the loading conditions. Yue and his co-workers (e.g. Xiao & Yue, 2014; Xiao et al., 2018, 2019) incorporated this fundamental solution into the classical BEMs for the analysis of the fracture mechanics in layered solids and found the solutions for many specific problems of interests in science and technology. The fundamental solution of infinite multilayered media is also suitable for the layered media of semi-infinite extent. In an infinite layered solid, the elastic modulus of the upper semi-infinite solid is given an extremely small value, such as $E_0=1\times10^{-10}$MPa and the Poisson's ratio of the solid $\nu_0=0.3$. In this way, the fundamental solution of a layered solid of semi-infinite extent is obtained.

2.2 The basic equations and numerical methods

The numerical method by Xiao, Yue & Zhao (2012) is further developed for evaluating the elastic fields of a non-homogeneous solid induced by a distributed load. In using the proposed numerical method for the analysis of a non-homogeneous halfspace exhibiting arbitrary variations in depth, the halfspace is discretized into a large number of homogeneous layers, as shown in Yue et al. (1999). It can be found that the development of the basic equations analyzing the elastic layered problem is relatively straightforward. These analyzing equations are presented for completeness.

As shown in Fig. 1, a non-homogeneous halfspace is subjected to internal loads in the *x*, *y* and/or *z* directions. The displacements and stresses at any points of the non-homogeneous solid are expressed as

$$u_i(Q) = \int_S u_{ik}^*(Q,P)\, t_k(P)\, dS \tag{1}$$

$$\sigma_{ij}(Q) = \int_S \sigma_{ijk}^*(Q,P)\, t_k(P)\, dS \tag{2}$$

where $u_{ik}^*(Q,P)$ and $\sigma_{ijk}^*(Q,P)$ are the fundamental solutions of the layered solid presented by Yue (1995); $u_{ik}^*(Q,P)$ are the *i*-th component of the displacement at the field point *Q* produced by the *k*-th component of a unit force applied at the source point *P*; $\sigma_{ijk}^*(Q,P)$ are the stresses at the field point *Q* produced by the *k*-th component of a unit force applied at the source point *P*; $t_k(P)$ is the traction at the source point *P*; the integral domain *S* is the loading area. It should be noted that the subscript *k* is a dummy index.

The loading area *S* is discretized into *ne* elements. The variable-node element similar to the one of boundary element methods (Xiao & Yue, 2014) is employed to discretize the loading area. In global and local coordinate systems, there are the following transform relationships of coordinate and traction values

$$x_i = \sum_{\alpha=1}^{4\text{ to }8} N_\alpha(\xi_1,\xi_2)\, x_i^\alpha \ ,\ t_i = \sum_{\alpha=1}^{4\text{ to }8} N_\alpha(\xi_1,\xi_2)\, t_i^\alpha \tag{3}$$

where $N_\alpha(\xi_1,\xi_2)$ is the shape function of the element and is presented in Appendix A.

Considering Eqs. (1) and (2) with (3), we have the following discretized forms

$$u_i(Q) = \sum_{e=1}^{ne} \sum_{\alpha=1}^{4\text{ to }8} t_k^\alpha(P) \int_{-1}^{1} \int_{-1}^{1} u_{ik}^*\left(Q, P(\xi_1,\xi_2)\right) N_\alpha(\xi_1,\xi_2)\, J(\xi_1,\xi_2)\, d\xi_1 d\xi_2 \tag{4}$$

$$\sigma_{ij}(Q) = \sum_{e=1}^{ne} \sum_{\alpha=1}^{4\text{ to }8} t_k^\alpha(P) \int_{-1}^{1} \int_{-1}^{1} \sigma_{ijk}^*\left(Q, P(\xi_1,\xi_2)\right) N_\alpha(\xi_1,\xi_2)\, J(\xi_1,\xi_2)\, d\xi_1 d\xi_2 \tag{5}$$

where *J* is the Jacobian determinant.

It is very important to obtain the accurate and efficient integration of the displacement and traction integral over the loading area. In Eqs. (4) and (5), three types of integrals exist and are calculated as follows:

(1) When the source point *Q* is not located at and is not close to the integral element, the integrals of Eqs. (4) and (5) are executed in the local coordinates and are calculated using the regular Gaussian quadrature.

(2) If the field point Q is located at the integral element, the integrand of Eq. (4) is of singularity $O\left(r^{-1}\right)$ and the integrand of Eq. (5) is of singularity $O\left(r^{-2}\right)$, where r is the distance between the points P and Q. The weakly singular integral of Eq. (4) is computed by applying an integration scheme based on a linear coordinate transformation (Beer et al., 2008; Gao & Davies, 2002) and the strongly singular integral of Eq. (5) is computed by using an indirect method.

(3) When the field point Q is not located on the loading area and the distance r between the points P and Q has a small value, the kernel functions u_{ik}^{*} and σ_{ijk}^{*} in Eqs. (4) and (5) have sharp variations. This type of integral is referred to as nearly singular integral, which will be discussed in the next section.

3 The subdivision scheme for nearly singular integral

3.1 Subdivision of an element

It has been found that the accuracy of calculating nearly singular integral is much related to the ratio of the length of an element to the distance from a field point to the element. As in Beer et al. (2008), an element may be further divided into sub-regions to solve nearly singular integral. In the ensuing, numerical integration techniques are developed to deal with nearly singular integral.

As shown in Fig. 2, the element is divided into several sub-regions. The number of sub-regions M_{ξ_1} in the direction ξ_1 and M_{ξ_2} in the direction ξ_2 is determined by

$$M_{\xi_1} = INT\left[\left(r/L\right)_{\min} / \left(r/L_{\xi_1}\right)\right] \tag{6}$$

$$M_{\xi_2} = INT\left[\left(r/L\right)_{\min} / \left(r/L_{\xi_2}\right)\right] \tag{7}$$

where the symbol *INT* denotes rounding off the results, r is the distance from the field source to the element, L_{ξ_1} and L_{ξ_2} are, respectively, the lengths of the element along the directions ξ_1 and ξ_2, $\left(r/L\right)_{\min}$ is the minimum value of r/L for obtaining the integration error 10^{-3} when the four Gaussian points is collocated. Erberwien et al. (2005) found that $\left(r/L\right)_{\min}$ = 0.79263, 1.67767 for $O\left(r^{-1}\right)$ and $O\left(r^{-2}\right)$, respectively.

The integration expressions on each element in Eqs. (4) and (5) can be further written as

$$\int_{-1}^{1}\int_{-1}^{1} f\left(\xi_1,\xi_2\right) d\xi_1 d\xi_2 = \sum_{s_1=1}^{M_{\xi_1}} \sum_{s_2=1}^{M_{\xi_2}} \left\{ \sum_{k=1}^{4}\sum_{l=1}^{4} f\left(\overline{\xi}_1,\overline{\xi}_2\right) \overline{J} \overline{w}_1 \overline{w}_2 \right\}_{s_1,s_2} \tag{8}$$

The relationships between the local coordinates $\left(\xi_1,\xi_2\right)$ and $\left(\overline{\xi}_1,\overline{\xi}_2\right)$ are

$$\xi_1=\frac{1}{2}\left(\xi_1^s+\xi_1^e\right)+\frac{\overline{\xi}_1}{M_{\xi_1}},\ \xi_2=\frac{1}{2}\left(\xi_2^s+\xi_2^e\right)+\frac{\overline{\xi}_2}{M_{\xi_2}} \tag{9}$$

where $\left(\xi_1^s,\xi_2^s\right)$ and $\left(\xi_1^e,\xi_2^e\right)$ define the starting and ending sides of the sub-region shown in Fig. 2. The Jacobian determinant $\overline{J}$ is given by

$$\overline{J}=\frac{\partial\xi_1}{\partial\overline{\xi}_1}\frac{\partial\xi_2}{\partial\overline{\xi}_2}=\frac{1}{M_{\xi_1}M_{\xi_2}} \tag{10}$$

3.2 The lengths of an element and the minimum distance r_{min}

The lengths of an element along the directions ξ_1 and ξ_2 can be calculated using the following

$$L_{\xi_1}=\int_{-1}^{1}\sqrt{\sum_{j=1}^{3}\left(\sum_{\alpha=1}^{4\text{ to }8}\frac{\partial N_\alpha}{\partial\xi_1}x_j^\alpha\right)_{\xi_2=0}^2}\,d\xi_1 \tag{11a}$$

$$L_{\xi_2}=\int_{-1}^{1}\sqrt{\sum_{j=1}^{3}\left(\sum_{\alpha=1}^{4\text{ to }8}\frac{\partial N_\alpha}{\partial\xi_2}x_j^\alpha\right)_{\xi_1=0}^2}\,d\xi_2 \tag{11b}$$

The lengths L_{ξ_1} and L_{ξ_2} expressed in Eq. (11) can be calculated using the Gaussian quadrature method. The iteration method developed by Gao & Davies (2002) can be used to calculate the minimum distance r_{min} from a field source to an element. The local coordinate origin of the element is chosen as a starting point for an iterating process. Taylor's theorem is used to obtain the r distance for the next step.

3.3 Numerical verification of the subdivision scheme

A numerical example is presented to verify the efficiency and accuracy of the proposed subdivision scheme. As shown in Fig. 3, the loading square-shaped area with a side length of a on the boundary surface of a homogeneous halfspace is considered. Assume that the elastic modulus E_0 and the Poisson's ratio ν=0.3. The uniform compressive traction f_z=1 is acted on the loading area, which is discretized using a 4-noded element. Using Eqs. (4) and (5), $u_z\left(0,0,z\right)$ and $\sigma_{zz}\left(0,0,z\right)$ can be expressed as

$$u_z\left(0,0,z\right)=\sum_{\alpha=1}^{4}\int_{-1}^{1}\int_{-1}^{1}u_{lz}^{*}\left(Q\left(0,0,z\right),P\left(\xi_1,\xi_2\right)\right)N_\alpha\left(\xi_1,\xi_2\right)J\left(\xi_1,\xi_2\right)d\xi_1 d\xi_2 \tag{12}$$

$$\sigma_{zz}\left(0,0,z\right)=\sum_{\alpha=1}^{4}\int_{-1}^{1}\int_{-1}^{1}\sigma_{ijz}^{*}\left(Q\left(0,0,z\right),P\left(\xi_1,\xi_2\right)\right)N_{\alpha}\left(\xi_1,\xi_2\right)J\left(\xi_1,\xi_2\right)d\xi_1 d\xi_2 \tag{13}$$

In the following, the numerical results will be compared with the closed-form solution presented by Xiao & Yue (2013).

Fig. 4a illustrates the variation of the relative errors of $u_z\left(0,0,z\right)E_0/f_z a$ with the number of sub-regions of an element at different z value. Using Eq. (6), $M=M_{\xi_1}=M_{\xi_2}=79$ for the integration error 10^{-3} at z/a=0.01. It can be found that the relative error of $u_z\left(0,0,z/a=0.01\right)E_0/f_z a$ decreases rapidly with M increasing and is equal to 0.02349271 for M=19. Correspondingly, at z/a=0.01 the numerical result $u_z\left(0,0,z\right)E_0/f_z a$=1.01617 whereas the accurate result $u_z\left(0,0,z\right)E_0/f_z a$=1.01593. It is obvious that the numerical result is much close to the accurate value. At z/a=0.1, the relative error of $u_z\left(0,0,z\right)E_0/f_z a$ decreases rapidly with M increasing and is equal to 0.00016408 for M=7 whereas M=7 using Eq. (6) for the integration error 10^{-3}. At z/a=0.5, the relative error of $u_z\left(0,0,z\right)E_0/f_z a$ is equal to 0.00072358 for M=1 whereas M=1 using Eq. (6) for the integration error 10^{-3}.

Fig. 4b illustrates the variation of the relative errors of $\sigma_{zz}\left(0,0,z\right)/f_z$ with the number of sub-regions of an element at different z values. At z/a=0.03 and 0.05, the relative errors of $\sigma_{zz}\left(0,0,z\right)/f_z$ decrease rapidly with M increasing and are, respectively, 0.13662 and 0.00347 for M=19. Correspondingly, at z/a=0.03 the numerical result $\sigma_{zz}\left(0,0,z\right)/f_z$=0.99847 whereas the accurate result $\sigma_{zz}\left(0,0,z\right)/f_z$=0.99983. It is obvious that the numerical result is much close to the accurate value. At z/a=0.03 and 0.05, M=55 and 33 respectively using Eq. (7) for the integration error 10^{-3}. At z/a=0.1 and 0.5, M=16 and 3 respectively using Eq. (7) for the integration error 10^{-3} and the relative error of $\sigma_{zz}\left(0,0,z\right)/f_z$ is equal to 0.59026 and 0.27×10^{-10} at M=16 and 3.

Table 1 presents the minimum number of M for the relative errors less than 1%. These data are much useful for discretizing the loading area. By comparing the numerical result with the closed-form solution, the accuracy of the proposed numerical quadrature can be evaluated and verified. Using the proposed method, the accurate numerical results can be obtained.

4. Parallelization of the proposed numerical method

Based on the expressions presented above, a computer program in Fortran has been written. In order to obtain the highly accurate numerical solution of an arbitrarily depth-heterogeneous elastic solid, the solid needs to be discretized into solids with a large number of layers in depth. Meanwhile, the loading area needs to be discretized into a fine mesh. All these induce a large scale of computations. In order to obtain the high efficiency and accuracy of computations, parallel computing can be implemented in the proposed numerical method.

OpenMP is a parallel programming model for shared memory and distributed shared memory multiprocessors (Chandra et al., 2001; Cunha et al., 2004). It allows parallelizing an application step-by-step, without concerns about how data and workload are distributed across multiple processors. Herein, we develop the parallelized computation for the proposed numerical method using OpenMP.

The proposed numerical method is characterized by a parallel nature. Since the computation of the coefficients of tractions in Eqs. (4) and (5) for each element is independent of the other, the loop iterations for elements can be safely performed concurrently. Here, a straight approach is to use OpenMP directives to parallelize the internal loop, which controls element iterations. These directives take the form of source code comments identified by the $OMP prefix and are simply ignored by a non-OpenMP compiler. Thus, the same source code can be used to compile a serial or parallel version of the application.

The application of OpenMP directives is demonstrated in the following reduced version of the code, listed in Table 2. In calculating the stresses on the loading surface and the fundamental solution, the similar parallelized computations are also applied.

5. Numerical results and verifications

5.1 General

In order to describe the variation of the shear modulus of elasticity in soils, Selvadurai & Katebi (2013) performed linear and exponential fittings for the data provided by Burland, Longworth, & Davis (1977), who investigated the depth variation of the geotechnical properties of Oxford clay. Katebi & Selvadurai (2013) further suggested that the variations of the shear modulus of the depth z were described by the following expressions

$$G(z) = G_0 e^{\lambda z} \tag{14}$$

$$G(z) = G_0 (1+mz) \tag{15}$$

where G_0 , λ and m are constant coefficients. It is further assumed that the Poisson's ratio keeps constant with depth.

In the following analysis, the segmental variations of the elastic shear modulus with depth are restricted in the following

$$G(z)=G_0e^{\lambda z},\ z\le d \text{ and } G(z)=G_0e^{\lambda d},\ z>d \tag{16}$$

$$G(z)=G_0(1+mz),\ z\le d \text{ and } G(z)=G_0(1+md),\ z>d \tag{17}$$

It means that the elastic shear modulus of the solid varies with depth for $z\le d$ and keeps constant for $z>d$.

5.2 Example 1: non-homogeneous halfspace subjected to uniform circular load

The first example given below is to validate numerically the solutions of the non-homogeneous halfspace subjected to the internal loads. The classical result of Katebi & Selvadurai (2013) is used for comparison purpose. By using the integral transform technique, Katebi & Selvadurai (2013) presented an exact analysis of stresses and displacements in a non-homogeneous elastic halfspace subjected to internal uniform circular loads along the z direction (radius $r=a$). For a non-homogeneous solid with an exponential variation of the shear modulus described in Eq. (16), there are the following conditions: Poisson's ratio $v=0.5$, the loading depth $h=a$ and the thickness of the nonhomogeneous layer $d=a$.

For $z\le d$, the non-homogeneous solid is closely approximated by n bonded layers of elastic homogeneous media. Each layer has the thickness equal to d/a and the shear modulus is equal to $G(z)$ at the bottom depth of this layer, i.e., for the i-th layer, $z=id/n$ (i=1,2,3,…,n). A homogeneous halfspace is bonded to the non-homogeneous solid with the thickness d. Fig. 5 illustrates an approximation of the continuous depth variation of the shear modulus by a large number of piece-wisely homogenous layers, where $\lambda=2$ and $n=100$. It can be found that a close approximation of the shear modulus variation can be obtained using a large number of n.

As shown in Fig. 6, the circular loading area is discretized into 180 eight-noded elements and 573 nodes. We compare the present results with those given by Katebi & Selvadurai (2013). The four cases $\lambda=0.5,1,2,3$ are analyzed using the layered approximations. Table 3 shows the vertical displacement at the point $(x,y,z)=(0,0,0)$. It can be found that the layered approximation ($n=100$) results in excellent results for the vertical displacement at the point. For $\lambda=0.5,1,2,3$, the absolute error between the results of the two methods are equal to 0.000901, 0.000277, 0.0006391 and 0.000733, respectively. It should be noted that the absolute error between the vertical displacements of a homogeneous halfspace for the point $(x,y,z)=(0,0,0)$ for these two methods is 0.00043.

The example above is further analyzed to demonstrate the efficiency of the proposed procedure by comparing with results from the commercial finite element software ABAQUS. To make sure the high accuracy of results from the software, the fine FEM mesh with 12336 elements and 13549 nodes are employed. For λ=0.5,1,2,3, the vertical displacement at the point (x,y,z)=(0,0,0) are, respectively, 0.219219, 0.132187, 0.048264 and 0.017920 and the corresponding absolute errors are 0.002377, 0.002530, 0.000745 and 0.000204 respectively. In our numerical simulation, only 180 elements and 573 nodes are used and the results with high accuracy can be obtained. Hence, the proposed procedure has a high efficiency in analyzing the behavior of vertically heterogeneous solids under the action of internal loads.

Results also show that the accurate results can be obtained using the numerical method together with the layered discretization technique. In the ensuing, we will use the proposed numerical method for the analysis of the non-homogeneous solid subjected to internal rectangular loading. It should be pointed out that all numerical results are presented in non-dimensional forms.

5.3 Example 2: non-homogeneous halfspace subjected to uniform rectangular load

The second example is designed to illustrate the numerical solutions of a point much close to the loading area. As shown in Fig. 1, the rectangular loading area is chosen to analyze the behavior of a non-homogeneous elastic solid, which has an exponential variation of the shear modulus described in Eq. (16). Assume that b=1.5a, d=a and h=a. The loading area is subjected to the vertical load f_z.

In order to obtain highly accurate numerical results, we choose four discretization meshes using eight-noded elements. Fig. 7 shows the Mesh 1 with 150 elements and 501 nodes. For simplicity, only the results along the vertical axis passing the corner (x, y, z) = (b, a, z) of the rectangular loading area are presented. Assume that the Poisson's ratio of the non-homogeneous solid λ=0.3. Fig. 8 illustrates the variation of horizontal and vertical displacements induced by f_z for four meshes, which are similar to ones shown in Fig. 7. The displacements are non-smoothly continuous across the loading surface. It can be found that all the four meshes can obtain good results for three displacement components, which are in very good agreement with the variation property mentioned above.

According to the property of the fundamental solution, the stresses vary sharply when the points are very close to the loading plane. Fig. 9 presents the variation of σ_{zz} induced by f_z for the points close to the loading plane for four meshes. The three points with a distance of 0.007a, 0.005a and 0.003a above or below the loading surface have almost the same results for Meshes 3

and 4. However, the point with a distance of 0.001a above or below the loading surface has different values for Meshes 3 and 4.

Xiao & Yue (2013) found that the loading f_z causes a jump discontinuity of the vertical stress σ_{zz} across the loading surface and the jump at the corner of the rectangular loading area is equal to 0.25f_z. For two points with a distance of 0.003a from the loading surface, the jumps at the corner are, respectively, 0.252497f_z and 0.248901f_z for Meshes 3 and 4 and have the absolute errors of 0.002497f_z and 0.001099 f_z. Thus, we choose Mesh 4 to perform the following analysis and present the results of points with a distance greater than or equal to 0.003a from the loading surface.

5.4 Example 3: Efficiency of the parallelization method

The third example is designed to compare the CPU times based on the serial and parallel algorithms. Listed in Table 4 are the CPU times for calculating the stresses and displacements at one point for Meshes 1, 2 and 3, which are used in analyzing Example 2. For each mesh, the heterogeneous layer is discretized into 50 and 100 discrete layers. As can be observed, the parallel algorithm is much faster than the serial algorithm, in particular when the number of the points to be analyzed is very large. More specifically, for the given mesh and the same number of discrete layers, the parallel algorithm is about 14 times faster than the serial algorithm, and for a given mesh, the case of 50 homogeneous discrete layers is about 3 times faster than the case of 100 discrete layers case using the two algorithms.

6. Numerical results and analyses of new applications

6.1 The elastic fields for an exponential variation of the shear modulus

It is assumed that the non-homogeneous solid has an exponential variation of the shear modulus in Eq. (16) and the Poisson's ratio of the non-homogeneous solid ν=0.3. The dimension of the rectangular loading area b=1.5a. The non-homogeneous solid with a thickness of d is discretized into 100 layers of homogeneous media with different values of the shear modulus according to the depth.

6.1.1 Results of the horizontal and vertical loads f_x, f_z for different λ

Consider now the influence of different λ for the horizontal and vertical loads at h=a. For simplicity, only the results along the vertical axis passing the corner (b, a, d) of the rectangular loading area are presented. Figs. 10 and 11 respectively give the values of the three displacements and six stresses induced by the vertical load f_x concentrated on the rectangular

area. Figs. 12 and 13 respectively give the values of the three displacements and six stresses induced by the vertical load f_z concentrated on the rectangular area. From these figures, we can have the following observations:

(1) The displacements and stresses in the non-homogeneous solid induced by f_x and f_z are different for different λ values (λ=0,0.5,1,1.5,2,2.5,3). The three displacements (u_x, u_y, u_z) are continuous across the loading plane.

(2) The absolute values of u_x and u_y induced by f_x decrease with λ increasing. The maximum values of u_x and u_y appear at the loading plane. For λ=0,0.5,1,1.5,2,2.5,3, the maximum values of $u_x(b,a,z)G_0 / f_x a$ are, respectively, 0.41731, 0.26689, 0.16901, 0.10617, 0.06627, 0.04114 and 0.02543. Usually, u_z induced by f_x is negative above the loading plane and is positive below the loading plane.

(3) The absolute values of u_x and u_y induced by f_z decrease with λ increasing. The maximum values of u_z appear at the loading plane. For λ=0,0.5,1,1.5,2,2.5,3, the maximum values of $u_z(b,a,z)G_0 / f_z a$ are, respectively, 0.43045, 0.26556, 0.16339, 0.10027, 0.0614, 0.03753 and 0.0229. With the distance to the loading plane increasing, the u_z values decrease.

(4) The vertical load f_x causes an obvious jump discontinuity of σ_{xz} and σ_{yz} for all the non-homogeneous solid with different λ and peak values of σ_{xx}, σ_{xy}, σ_{yy} and σ_{zz} appear at the loading plane. With λ increasing, the absolute values of σ_{xx} and σ_{xy} induced by f_x increase for $z>a$ and decrease for $z<a$. With λ increasing, the absolute values of σ_{xz} and σ_{yz} induced by f_x decrease for $z>a$ and increase for $z<a$.

(5) the stresses (σ_{yy} and σ_{zz}) induced by f_z has a variation similar to σ_{xx} with λ and z. For $z>a$ and $z<a$, σ_{xy} induced by f_z has a variation similar to σ_{xx} for $z<a$. σ_{xz} and σ_{yz} have the same variations with depth. With λ increasing, σ_{xz} and σ_{yz} decrease for $z<a$ and increase for $z>a$.

(6) The vertical load f_z causes a jump discontinuity of σ_{xx}, σ_{xy}, σ_{yy} and σ_{zz} for all the non-homogeneous solids with different λ. Besides, σ_{xz} and σ_{yz} tend to relative small values with the distance to the loading plane decreasing. With λ increasing, the absolute values of σ_{xx} induced by f_z increase for $z>a$. However, with λ increasing, σ_{xx} increase in the shallow zone of

$z<a$ and decrease in the deep zone of $z<a$. σ_{yy} and σ_{zz} induced by f_z has a variation similar to σ_{xx} with λ and z. For $z>a$ and $z<a$, σ_{xy} induced by f_z has a variation similar to σ_{xx} for $z<a$. σ_{xz} and σ_{yz} have the same variations with depth. With λ increasing, σ_{xz} and σ_{yz} decrease for $z<a$ and increase for $z>a$.

6.1.2 Results of the vertical load f_z for $h=a$ and $z=0.75a$

Consider now the loading depth $h=a$ and present the results at $z=0.75a$. Let us take the calculating area: $-3 \le x/a \le 3$, $-2 \le y/a \le 2$ and $z=0.75a$. Figs. 14 and 15 respectively present the contours of displacements and stresses on the calculating area by the vertical load f_z. Because of symmetry, the values of displacements and stresses are given only for $0 \le x/a \le 3$ and $-2 \le y/a \le 2$. From these figures, we can have the following observations:

(1) The displacement u_x is antisymmetric with respect to the y axis on a horizontal plane and u_x is zero along the y axis. The displacements (u_y, u_z) are symmetric with respect to the y axis on a horizontal plane. On the calculating area, the maximum absolute value of $u_x(x,y,0.75a)G_0/f_z a$ is 0.01285. The maximum and minimum values of $u_y(x,y,0.75a)G_0/f_z a$ are, respectively, 0.0167 and -0.0167. And the maximum and minimum values of $u_z(x,y,0.75a)G_0/f_z a$ are, respectively, 0.46529 and 0.11812.

(2) The three normal stresses (σ_{xx}, σ_{yy}, σ_{zz}) are symmetric with respect to the y axis. The minimum values of $\sigma_{xx}(x,y,0.75a)/f_z$ and $\sigma_{yy}(x,y,0.75a)/f_z$ are -0.08707 and -0.09176, respectively and the maximum values of these components are -0.00766 and -0.01634, respectively. Because the calculating area is located above the loading area, i.e., $z=0.75a$, σ_{zz} is a tensile stress in a part of the area. The maximum and minimum values of $\sigma_{zz}(x,y,0.75a)/f_z$ are 0.18215 and -0.08957, respectively.

(3) Among the shear stresses (σ_{xy}, σ_{yz} and σ_{xz}), σ_{xy} and σ_{xz} are antisymmetric with respect to the y axis, and σ_{yz} is symmetric with respect to the y axis. The maximum absolute values of $\sigma_{xy}(x,y,0.75a)/f_z$ and $\sigma_{xz}(x,y,0.75a)/f_z$ are 0.04506 and 0.20127, respectively. The minimum value of $\sigma_{yz}(x,y,0.75a)/f_z$ is -0.22792.

6.1.3 Results of the vertical load f_z for different h

Consider now the case of different loading depths for λ=0.1. For simplicity, only the results along the vertical axis passing the corner (b, a, h) of the rectangular loading area are presented. Figs. 16 and 17 respectively illustrate the variations of the three displacements and six stresses induced by the vertical load f_z with the loading depth h. From these figures, we can have the following observations:

(1) The displacements u_x and u_y decrease with the depth h increasing. The maximum values of $u_x(b,a,z)G_0 / f_z a$ are, respectively, 0.1054, 0.06654, 0.04677, 0.03569 and 0.02917 for d=0, 0.25, 0.5, 0.75, 1. And the maximum values of $u_y(b,a,z)G_0 / f_z a$ are respectively 0.09024, 0.05335, 0.03647, 0.03569 and 0.022294 for d=0, 0.25, 0.5, 0.75, 1. With the depth h increasing, the maximum values of u_x and u_y appear at deeper positions. The u_z values increase for $z \geq h$ whilst the u_z values decrease for $z<h$ except for h=0. The maximum values of $u_z(b,a,z)G_0 / f_z a$ are, respectively, 0.43368, 0.42513, 0.41493, 0.40333 and 0.3909 for d=0, 0.25, 0.5, 0.75, 1.

(2) For different loading depths, the jumps of σ_{xx}, σ_{xy}, σ_{yy} and σ_{zz} always appear across the loading plane and the maximum absolute values of σ_{xz} and σ_{yz} always appear at the loading plane. The jumps of $\sigma_{xx}(b,a,z)/f_z$, $\sigma_{xy}(b,a,z)/f_z$, $\sigma_{yy}(b,a,z)/f_z$ and $\sigma_{zz}(b,a,z)/f_z$ at the corner of the rectangular loading area are equal to about 0.107, 0.114, 0.106 and 0.25 respectively for different loading depths. And the values of these stresses at the points close to the boundary surface z=0 are -0.1808, -1900, -0.2036 and -0.25, respectively.

(3) With the distance from the point to the loading plane increasing, the absolute values of σ_{xx}, σ_{yy} and σ_{zz} decrease below the loading plane and increase above the loading plane. However, with the distance from the point to the loading plane increasing, the absolute values of σ_{xy} decrease below and above the loading plane. The maximum absolute values of σ_{xz} and σ_{yz} appear at the loading plane and increase with loading depth h increasing.

6.2 Comparison for two different distributions of the shear modulus

Eqs. (16) and (17) present two different distributions of shear modulus for a non-homogenous halfspace. In order to compare their results, we analyze the displacements induced by f_z for λ=0.1 and m=2λ. Assume that the Poisson's ratio of the non-homogeneous solid ν=0.3. The vertical load f_z is located at z=0. For the two non-homogeneous halfspaces, the shear moduli

have the same value at about d=12.564a. The shear modulus of a non-homogeneous halfspace varies with depth for $z<d$ and keeps constant for $z \geq d$.

To provide a better estimate of the relative influence of elastic non-homogeneity on the displacements of the solid, the ratio of displacements in a non-homogeneous solid to that in a homogeneous solid has been evaluated and is presented in Fig. 18 for both linear and exponential variations. As would be expected, the displacements are much lower for the exponential variation than for the linear variation of the shear modulus.

6.3 The influence of the Poisson's ratio of a non-homogeneous solid

In the above-mentioned analyses, it is assumed that the Poisson's ratio of the nonhomogeneous solid keeps constant along depth. Actually, the Poisson's ratio of the nonhomogeneous solid varies with depth. In order to provide an example application of the variation of Poisson's ratio with depth, a simple linear fit has been completed for the data by Pan (1985), who investigated the depth variation of the geotechnical properties of sand soil, clay loam, clay and soft soil. Pan (1985) showed that the Poisson's ratio increases with the depth z, although the variation is not necessarily linear. The ratios of increase in the Poisson's ratio were different for different types of soils. The variations of the elastic modulus and the Poisson's ratio for sand soil are presented as follows:

$$E(z) = E_0(1 + m_1 z) \tag{18}$$

$$v(z) = v_0(1 + m_2 z) \tag{19}$$

where E_0=53.09MPa, m_1=0.5065 and ν_0=0.3469, m_2=0.0123, and the SI unit of z is meters (m). The thickness of the sand soil is d=12m. For $z \geq d$, the elastic properties keeps constants, that is, $E(z \geq d) = E_0(1 + m_1 d)$ and $v(z \geq d) = v_0(1 + m_2 d)$. The numerical results for this variation are presented in this section.

It is assumed that the rectangular loading area is located at h=a. Let us consider b=1.5a and d=a. Here, only the results along the vertical axis passing the corner (b,a,z) of the rectangular loading area are presented. Figs. 19 and 20 respectively give the values of the three displacements and six stresses induced by the vertical load f_z concentrated on the rectangular area for two cases: ν=ν_0 (case a) and $v = v_0(1 + m_2 z)$ (case b). From these figures, we can have the following observations:

(1) With the comparison of the displacements of cases a and b, the variations of the Poisson's ratio with depth exert an obvious influence on all the three displacements in

nonhomogeneous media. The values of the three displacements for case *a* become smaller than that for case *b* at a given depth.

(2) The variations of the Poisson's ratio with depth exert a different influence on different stress components. At a given depth, the σ_{xx} for case *a* is larger than that for case *b* and has different variations for two cases with depth for $z \le a$. For $z>a$, the σ_{yy} of case *b* is larger than that of case *a* whilst for $z<a$, the σ_{yy} of case *b* is smaller than that of case *a*. For $z>a$ and $z<a$, the σ_{zz} of case *b* become smaller than that of case *a*.

(3) The shear stresses σ_{xz} and σ_{yz} have a similar variation between cases *a* and *b*. In the neighborhood of the loading plane, the concentration of the stresses σ_{xz} and σ_{yz} for case *b* becomes less obvious than that for case *a*. The variation of the shear stress σ_{xy} is different from that of σ_{xz} and σ_{yz}. For $z>a$ and $z<a$, the σ_{xy} of case *b* is smaller than that of case *a*.

7. Conclusions

This paper presents an effective numerical method for the analysis of the displacement and stresses corresponding to internal distributed loads of a non-homogeneous isotropic elastic halfspace. Numerical verification shows that the proposed numerical method can obtain accurate results, especially for the point close to the loading area. The displacements and stresses induced by the horizontal and vertical loadings are presented in details. The non-homogeneous halfspace analyzed can have their shear modulus exhibiting exponential and linear variations in depth and keeping constant in lateral directions. Furthermore, the variation of the Poisson's ratio along a vertical direction is also considered. The internal rectangular loading of an elastic halfspace can serve as a useful model for analyzing the internal loading of geologic media. The numerical method can be also used to analyze a non-homogeneous halfspace where the elastic properties exhibit arbitrary variations with depth.

Acknowledgements

The work presented in this paper was supported by the National Natural Science Foundation of China (Grant No. 41672291) and SDUST Research Fund (2015TD-JH104). In addition, we would also thank Prof. A.P.S. Selvadurai of McGill University, Canada, for supplying the data of their research in Table 3. The authors are grateful to the four reviewers for their valuable comments and suggestions, which have greatly improved the manuscript presentation.

Appendix A

The eight shape functions of the element can be written as

$$N_\alpha(\xi_1,\xi_2)=\frac{1}{2}\left(1-\xi_1^2\right)\left(1+\xi_2^\alpha\xi_2\right)\quad(\alpha=5,7)$$

$$N_\alpha(\xi_1,\xi_2)=\frac{1}{2}\left(1-\xi_2^2\right)\left(1+\xi_1^\alpha\xi_1\right)\quad(\alpha=6,8)$$

$$N_1(\xi_1,\xi_2)=N_1^*-\frac{1}{2}(N_8+N_5)$$

$$N_2(\xi_1,\xi_2)=N_2^*-\frac{1}{2}(N_5+N_6)$$

$$N_3(\xi_1,\xi_2)=N_3^*-\frac{1}{2}(N_6+N_7)$$

$$N_4(\xi_1,\xi_2)=N_4^*-\frac{1}{2}(N_7+N_8)$$

where $N_\alpha^*(\xi_1,\xi_2)=\frac{1}{4}\left(1+\xi_1^\alpha\xi_1\right)\left(1+\xi_2^\alpha\xi_2\right)$ (α=1,2,3,4). ξ_β^α (β=1, 2) denotes the local coordinates in the β direction at node α. The shape functions of a variable-node element are obtained by letting the functions of the disappearing midside nodes be zero.

References

Abbiss, C. P. (1979). A comparison of the stiffness of the chalk at Mundford from a seismic survey and a large-scale tank test. *Géotechnique, 29*, 461-468.

Beer, G., Smith, I., & Duenser, C. (2008). *The boundary element method with programming for engineers and Scientists*. *Springer Wien: New York.*

Booker, J. R., Balaam, N. P., & Davis, E. H. (1985). The behavior of an elastic non-homogeneous half-Space. Part I: line and point loads. *International Journal for Numerical and Analytical Methods in Geomechanics, 9*, 353-367.

Burland, J. B., Longworth, T. I., & Moore, J. F. A. (1977). A study of ground movement and progressive failure caused by a deep excavation in Oxford Clay. *Géotechnique*, *27*, 557-59*1*.

Buxboim, A., Rajagopal, K., Brown, A. E. X., & Discher, D. E. (2010). How deeply cells feel: methods for thin gels. *Journal of Physics: Condensed Matter,* 22, 194116.

Chandra, R., Dagum, L., Kohr, D., Maydan, D., McDonald, J., & Menon, R. (2001). *Parallel programming in OpenMP*. *Academic Press*: *New York.*

Cunha, M. T. F., Telles, J. C. F., Coutinho, A. L. G. A., & Panetta, J. (2004). On the parallelization of boundary element codes using standard and portable libraries. *Engineering Analysis with Boundary Elements, 28,* 893-902.

Chen, W. T. (1971). Computation of the stresses and displacements in a layered elastic medium. *International Journal of Engineering Science, 9*, 775-800.

Doherty, J. P., & Deeks, J. A. (2003). Scaled boundary finite-element analysis of a non-homogeneous elastic half-space. *International Journal for Numerical Methods in Engineering, 57*, 955-973.

Erberwien, U., Duenser, C., & Moser, W. (2005). Efficient calculation of internal results in 2D elasticity BEM. *Engineering Analysis with Boundary Elements, 29*, 447-453.

Gao, X. W., & Davies, T. G. (2002). *Boundary element programming in mechanics*. *Cambridge: Cambridge University Press.*

Guo, N., & Zhao, J. D. (2016). 3D multiscale modeling of strain localization in granular media. *Computers and Geotechnics, 80,* 360-372.

Gibson, R. E. (1967). Some results concerning displacements and stresses in a non-homogeneous elastic half-space. *Géotechnique, 17*, 58-67.

Katebi, A., & Selvadurai, A. P. S. (2013). Undrained behavior of a non-homogeneous elastic medium: the influence of variations in the elastic shear modulus with depth. *Géotechnique, 63*, 1159-1169.

Marmo, F., & Rosati, L. (2016). A general approach to the solution of Boussinesq's problem for polynomial pressures acting over polygonal domains. *Journal of Elasticity, 122*, 75-112.

Marmo, F., Sessa, S., & Rosati, L. (2016). Analytical solution of the Cerruti problem under linearly distributed horizontal loads over polygonal domains. *Journal of Elasticity, 124*, 27-56.

Marmo, F., Toraldo, F., & Rosati, L. (2017). Transversely isotropic half-spaces subject to surface pressures. *International Journal of Solids and Structures, 104-105,35-49.*

Maloney, J. M., Walton, E. B., Bruce, C. M., & Van Vliet, K. J. (2008). Influence of finite thickness and stiffness on cellular adhesion-induced deformation of compliant substrata. *Physical Review E*, 78, 041923.

Merkel, R., Kirchgeßner, N., Cesa, C. M., & Hoffmann, B. (2007) Cell force microscopy on elastic layers of finite thickness. *Biophysical Journal* 2007; 93(9):3314-3332.

Pan, E. N. (1989). Static response of a transversely isotropic and layered half-space to general surface loads. *Physics of the Earth and Planetary Interiors*, *54*, 353-363.

Pan, E. N., Bevis, M., Han F., Zhou H., & Zhu R. (2007). Surface deformation due to loading of a layered elastic half-space: a rapid numerical kernel based on a circular loading element. *Geophys. J. Int. 171*, 11-24.

Pan, F. L. (1985). Effect of buried depth of soil layer on Poisson's ratio and lateral compressive stress to vertical compressive stress ratio. *China Civil Engineering Journal, 18,* 53-60.

Rajapakse, R. K. N. D., & Selvadurai, A. P. S. (1989). Torsion of foundations embedded in non-homogeneous soil in a weathered crust. *Géotechnique, 39,* 485-496.

Rostovtsev, N. A. (1964). On the theory of elasticity of a non-homogeneous medium. *Journal of Applied Mathematics and Mechanics, 28,* 601-611.

Selvadurai, A. P. S., Singh, B. M., & Vrbik, J. (1986). A Reissner-Sagoci problem for a nonhomogeneous elastic solid. *Journal of Elasticity, 16,* 383-391.

Stark, R. F., & Booker, J. R. (1997). Surface displacements of a nonhomogeneous elastic half-space subjected to uniform surface tractions. Part I: Loading on arbitrarily shaped area. *International Journal for Numerical and Analytical Methods in Geomechanics, 21,* 361-378.

Selvadurai, A. P. S., & Katebi, A. (2013). Mindlin's problem for an incompressible elastic half-space with an exponential variation in the linear elastic shear modulus. *International Journal of Engineering Science, 65,* 9-21.

Selvadurai, A. P. S. (2007). The analytical method in geomechanics. *Applied Mechanics Reviews, 60,* 87-106.

Xiao, H. T., & Yue, Z. Q. (2014). *Fracture mechanics in layered and graded solids: analysis using boundary element methods*. *De Gruyter: Berlin.*

Xiao, H. T., & Yue, Z. Q. (2013). Elastic Fields in two joined transversely isotropic media of infinite extent due to rectangular loading. *International Journal for Numerical and Analytical Methods in Geomechanics, 37,* 247-277.

Xiao, H. T., Yue, Z. Q., & Zhao, X. M. (2012). A generalized Kelvin solution based method for analyzing elastic fields in heterogeneous rocks due to reservoir water impoundment. *Computers and Geoscience, 43,* 126-136.

Xiao, S., Yue, Z. Q., & Xiao, H. T. (2018). Boundary element analysis of elastic fields in non-horizontally layered halfspace whose horizontal boundary subject to tractions. *Engineering Analysis with Boundary Elements, 95*, 105-123.

Xiao, S., Yue, Z. Q., & Xiao, H. T. (2019). Dual boundary element method for analyzing three-dimensional cracks in horizontally layered halfspaces. *Engineering Analysis with Boundary Elements, 104*, 135-147.

Xiao, S., Yue, Z. Q., & Xiao, H. T. (2019). Boundary element analysis of transversely isotropic bi-material halfspaces with inclined planes of isotropy and interfaces. *International Journal for Numerical and Analytical Methods in Geomechanics, 43*, 2599-2627.

Yue, Z. Q. (1995). On generalized Kelvin solutions in a multilayered elastics medium. *Journal of Elasticity, 40,* 1-43.

Yue, Z. Q., Yin, J. H., & Zhang, S. Y. (1999). Computation of point load solutions for geo-materials exhibiting elastic non-homogeneity with depth. *Computers and Geotechnics, 25*, 75-105.

Zhao, J. D., Jiang, M. J., Soga, K., & Luding, S. (2016). Micro origins for macro behavior in granular media. *Granular Matter*. *18*: 59.

Zhang, P. C., Liu, J., & Lin, G. (2016). Elastic displacement fields of multi-layered transversely isotropic materials under rectangular loads. *European Journal of Environmental and Civil Engineering,22,*1-29.

Zhang, P. C., Lin, G., Liu, J., & Wang, W. W. (2016). Response of multilayered transversely isotropic medium due to axisymmetric loads. *International Journal for Numerical and Analytical Methods in Geomechanics*, *40*, 827-864.

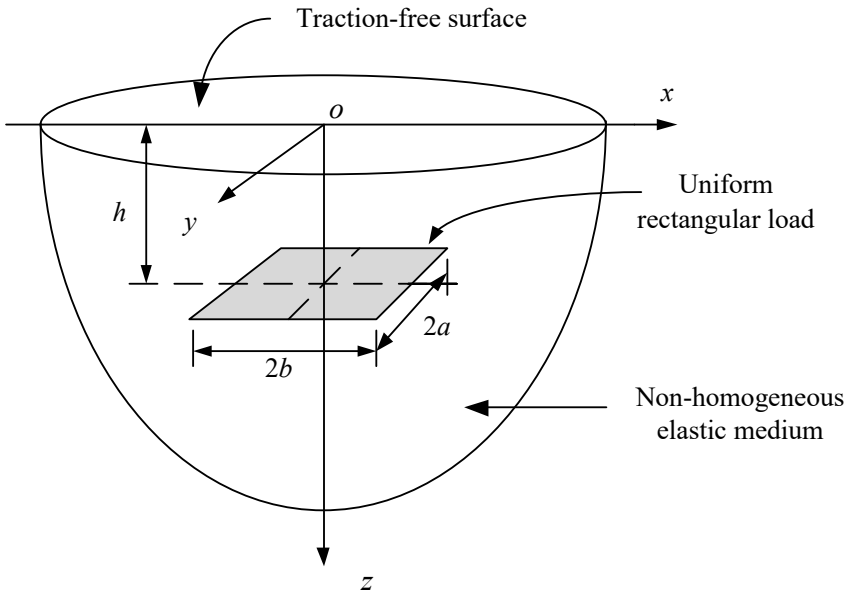

Fig.1 Uniform rectangular loads at the interior of a non-homogeneous elastic halfspace

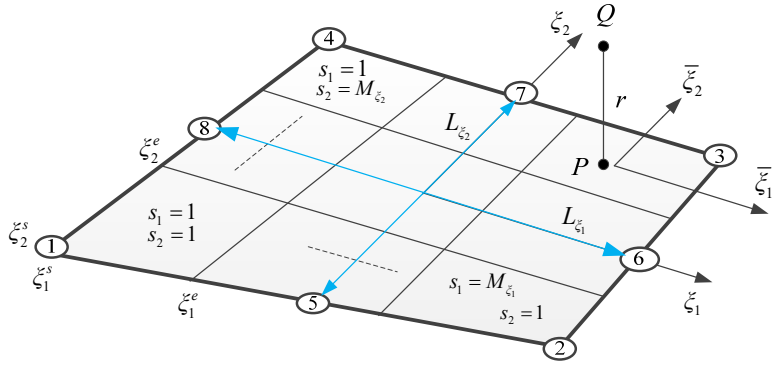

Fig. 2 Subdivision of a two-dimensional element

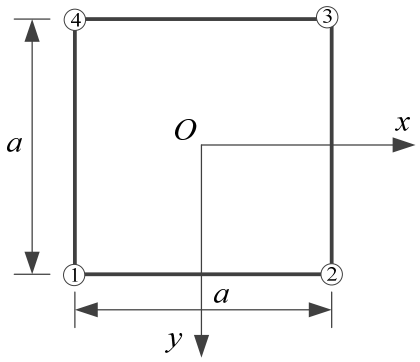

Fig. 3 Square-shaped loading area with a side length of a and one 4-node element

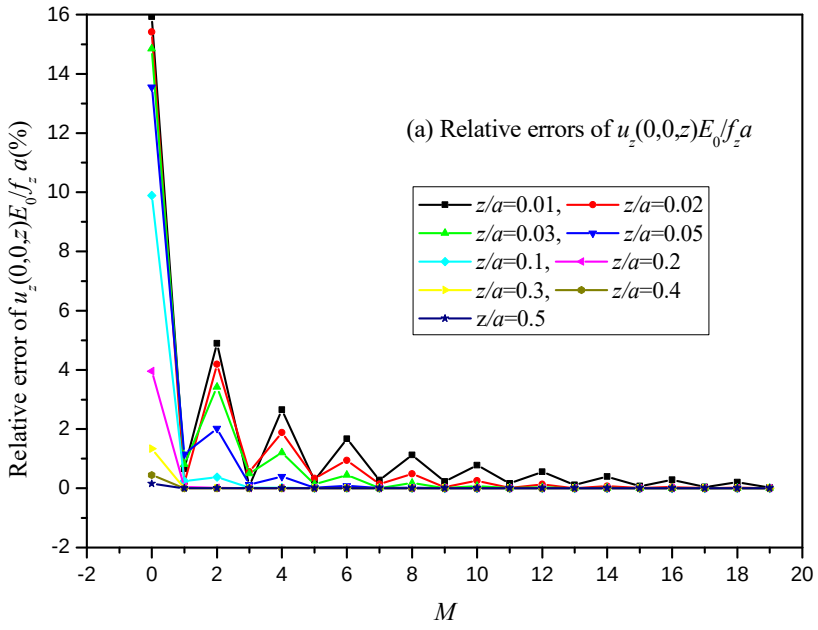

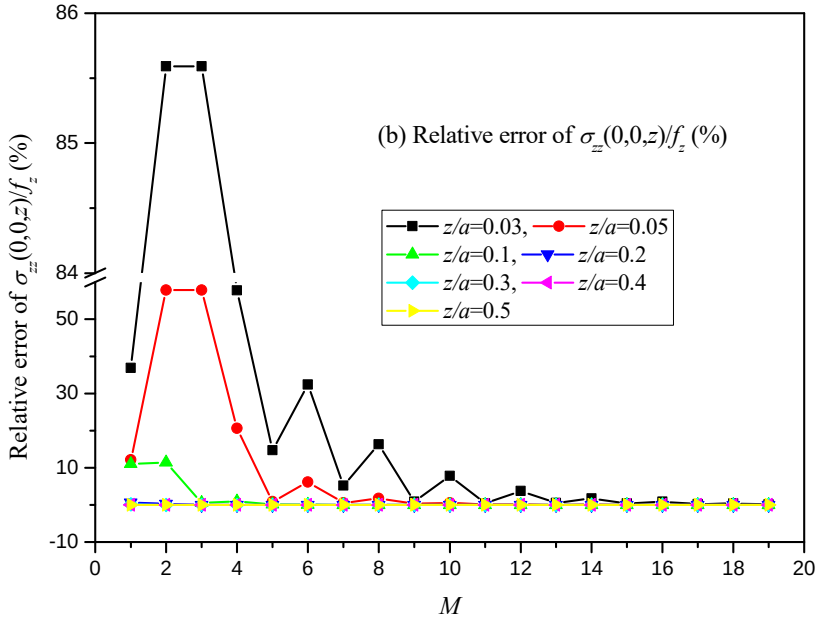

Fig.4 Variation of relative errors of the displacement and stress with the M value of sub-regions along the ξ_1 and ξ_2 directions

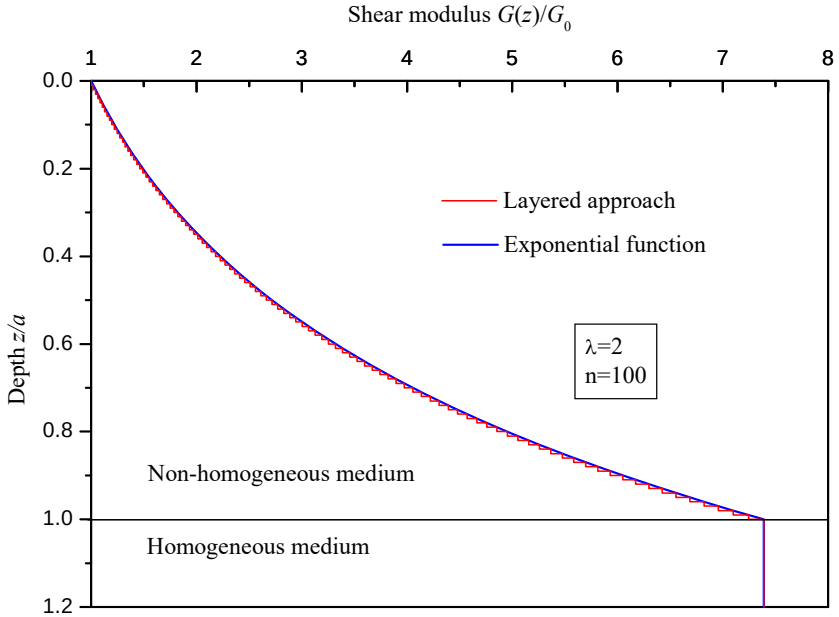

Fig. 5 Approximation of the continuous variation of the shear modulus by a system of 100 piece-wisely homogeneous layers

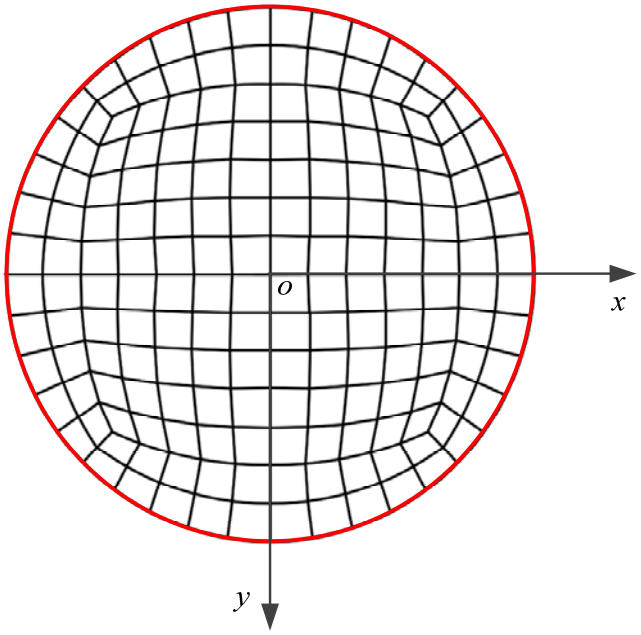

Fig. 6 Discretization mesh of the circular loading area (radius a) with 180 elements and 573 nodes

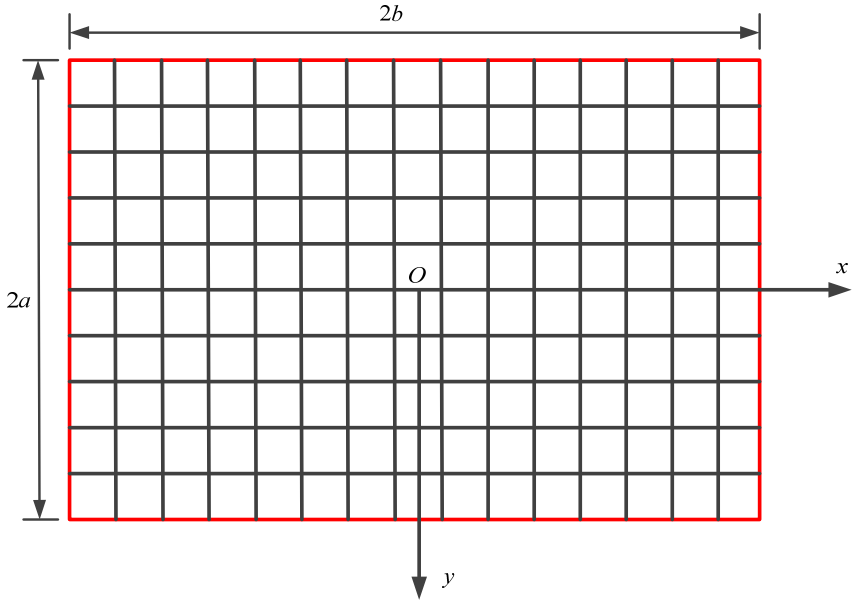

Fig. 7 Discretization mesh of the rectangular loading area with 150 elements and 501 nodes

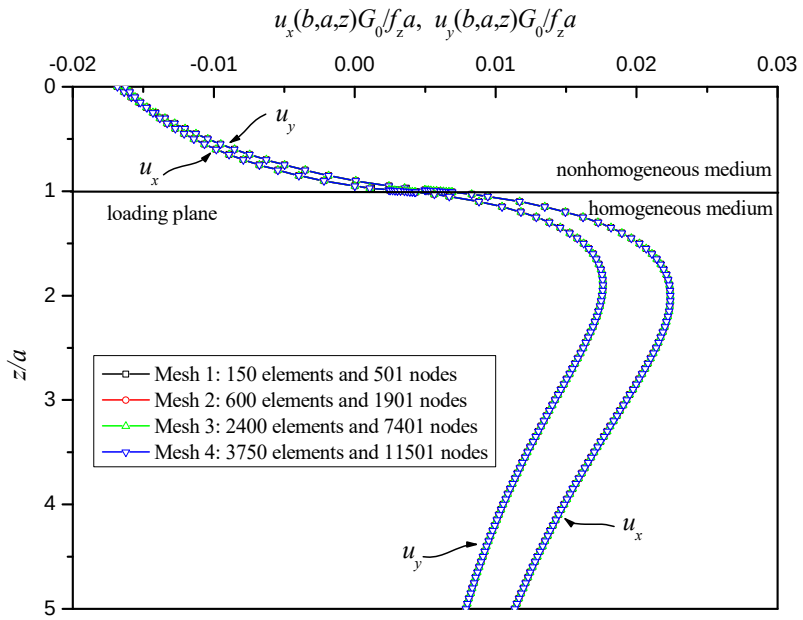

Fig. 8 Comparison of horizontal displacements for different meshes (λ=0.5)

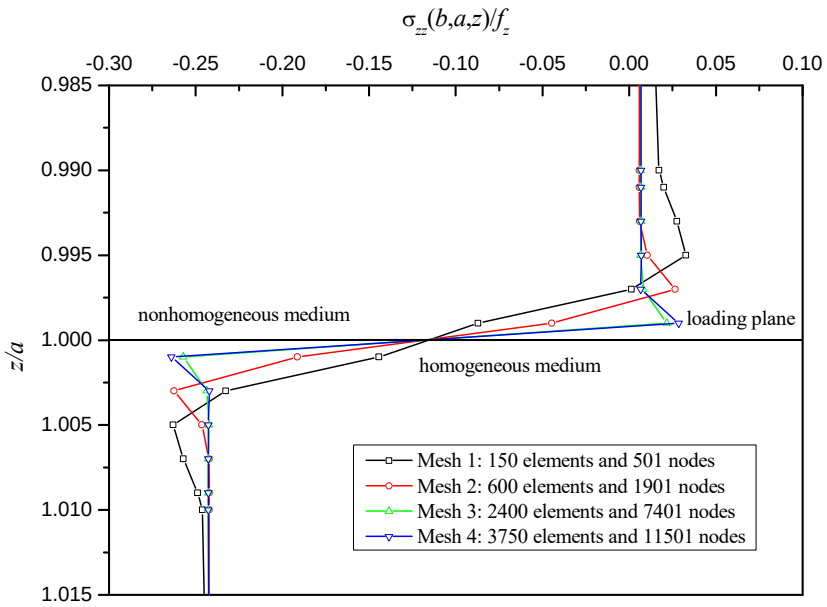

Fig. 9 Variation of vertical stress σ_{zz} at the points close to the loading plane for different meshes (λ=0.5)

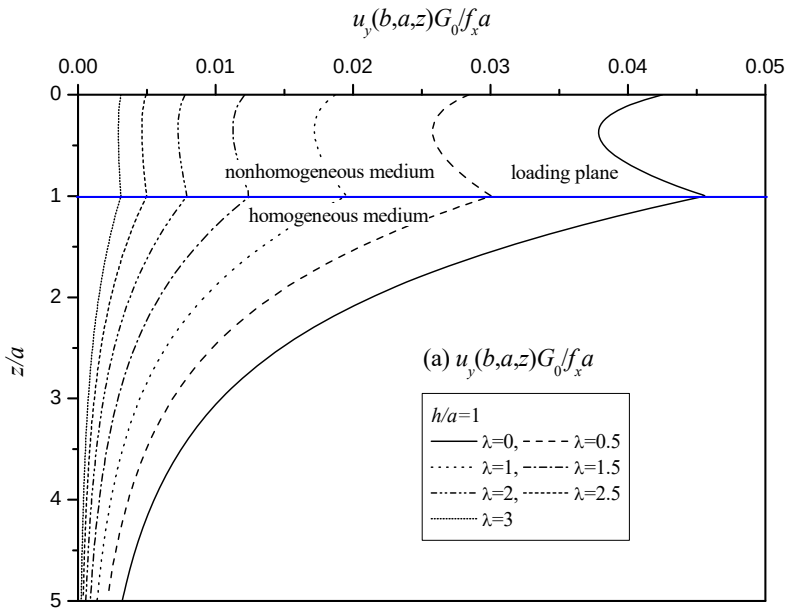
$u_y(b,a,z)G_0/f_x a$
0.00
0.01
0.02
0.03
0.04
0.05
0
1
2
3
4
5
z/a
nonhomogeneous medium
loading plane
homogeneous medium
(a) $u_y(b,a,z)G_0/f_x a$
h/a=1
λ=0, λ=0.5
λ=1, λ=1.5
λ=2, λ=2.5
λ=3

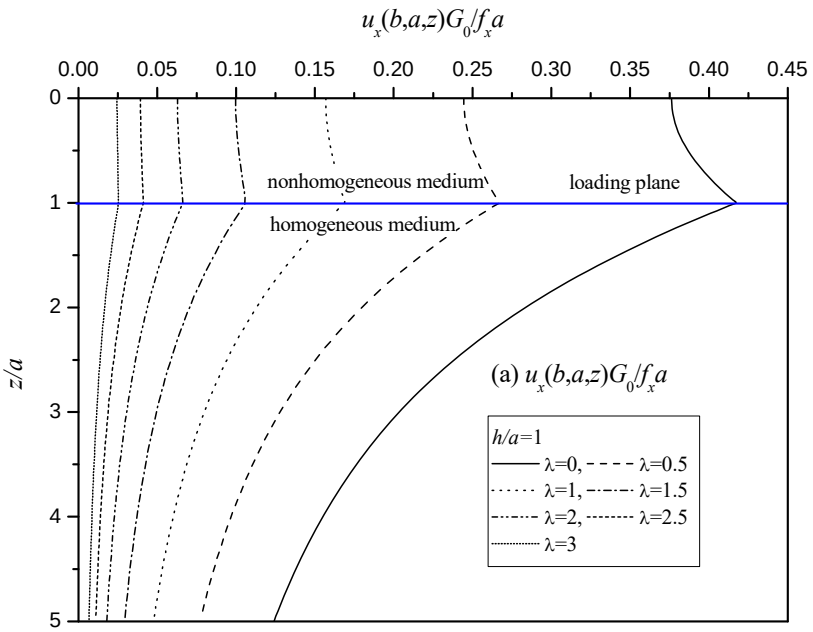
$u_x(b,a,z)G_0/f_x a$
0.00
0.05
0.10
0.15
0.20
0.25
0.30
0.35
0.40
0.45
0
1
2
3
4
5
z/a
nonhomogeneous medium
loading plane
homogeneous medium
(a) $u_x(b,a,z)G_0/f_x a$
h/a=1
λ=0, λ=0.5
λ=1, λ=1.5
λ=2, λ=2.5
λ=3

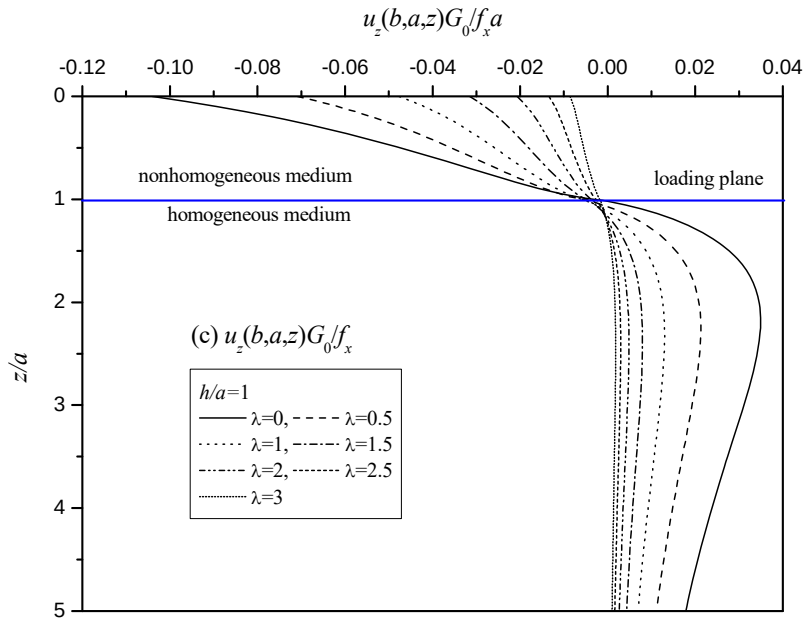

Fig.10 Variation of the displacement at the point (b, a, z) because of f_x located at h=a for different λ

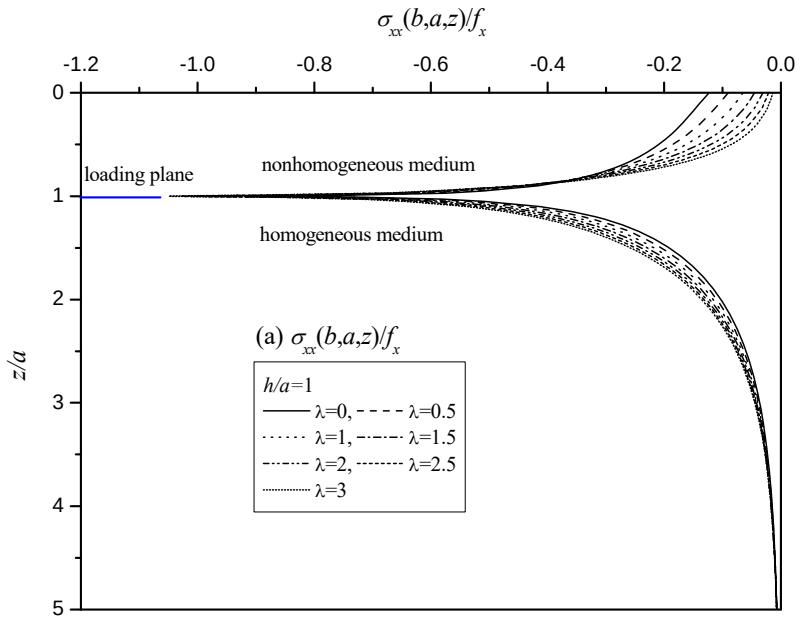

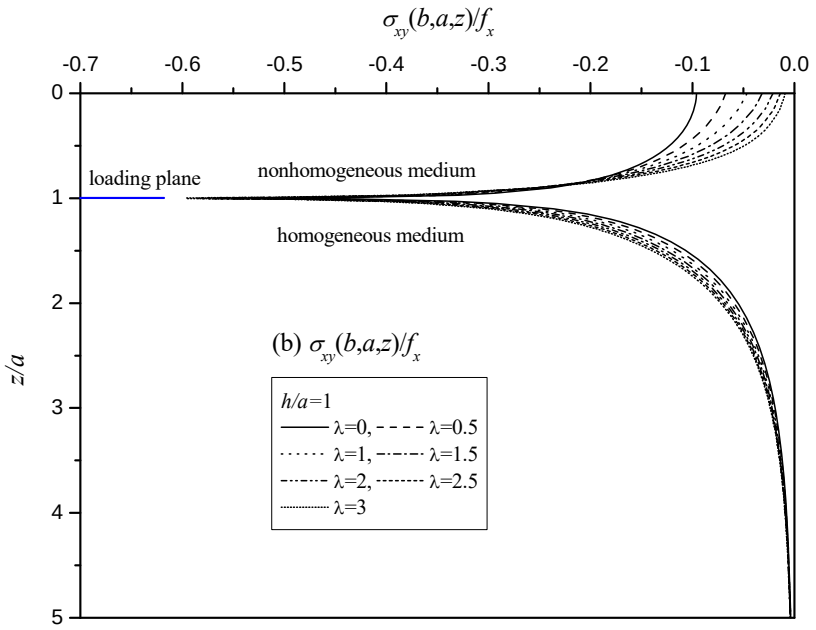
$\sigma_{xy}(b,a,z)/f_x$
-0.7
-0.6
-0.5
-0.4
-0.3
-0.2
-0.1
0.0
0
1
2
3
4
5
z/a
loading plane
nonhomogeneous medium
homogeneous medium
(b) $\sigma_{xy}(b,a,z)/f_x$
h/a=1
λ=0, λ=0.5
λ=1, λ=1.5
λ=2, λ=2.5
λ=3

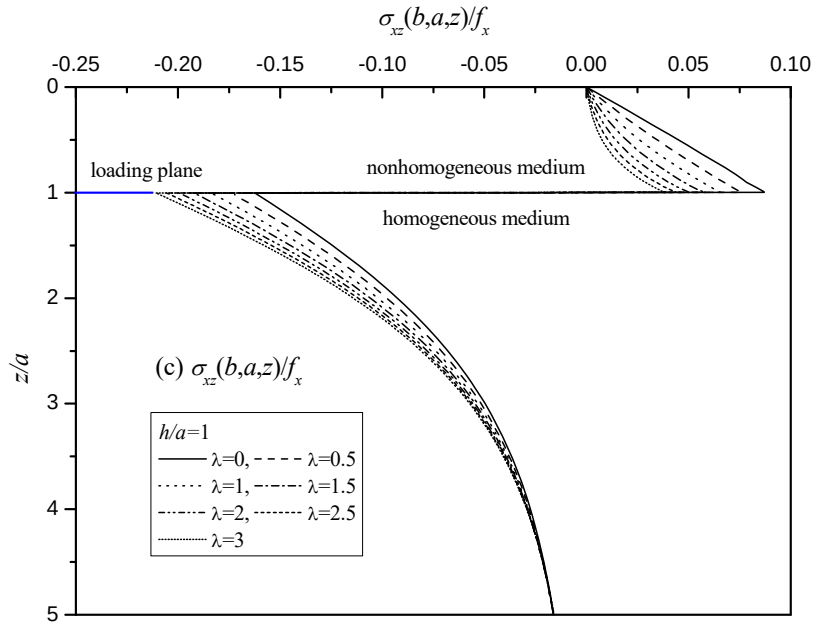
$\sigma_{xz}(b,a,z)/f_x$
-0.25
-0.20
-0.15
-0.10
-0.05
0.00
0.05
0.10
0
1
2
3
4
5
z/a
loading plane
nonhomogeneous medium
homogeneous medium
(c) $\sigma_{xz}(b,a,z)/f_x$
h/a=1
λ=0, λ=0.5
λ=1, λ=1.5
λ=2, λ=2.5
λ=3

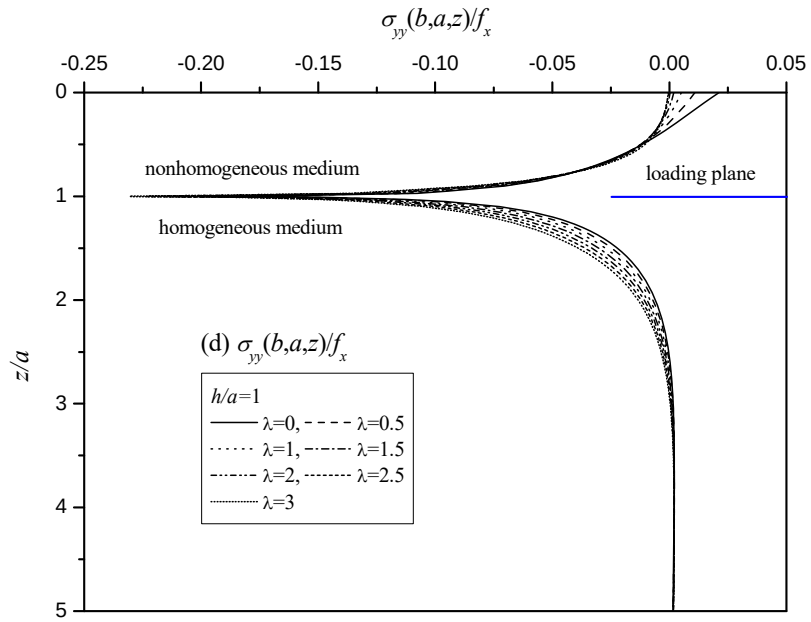
$\sigma_{yy}(b,a,z)/f_x$
-0.25
-0.20
-0.15
-0.10
-0.05
0.00
0.05
0
1
2
3
4
5
z/a
nonhomogeneous medium
loading plane
homogeneous medium
(d) $\sigma_{yy}(b,a,z)/f_x$
h/a=1
λ=0, λ=0.5
λ=1, λ=1.5
λ=2, λ=2.5
λ=3

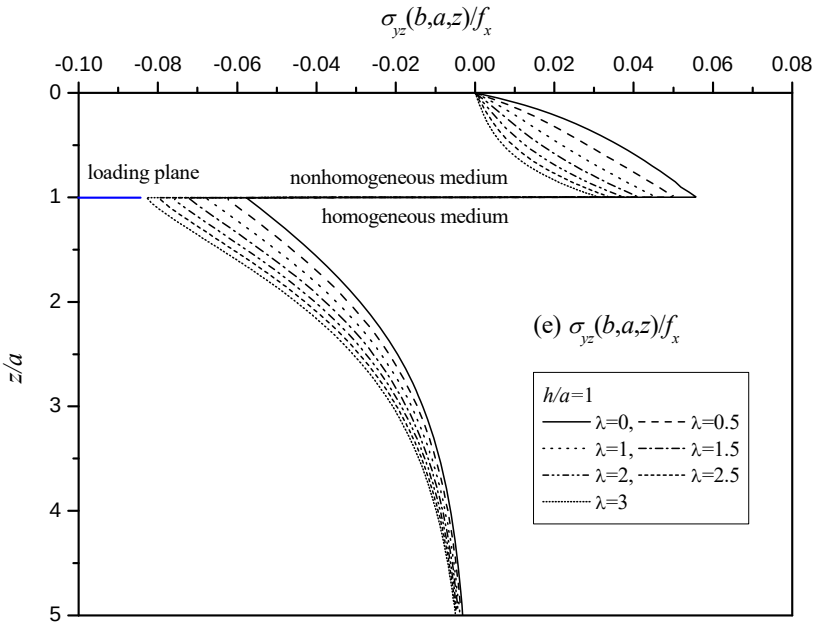
$\sigma_{yz}(b,a,z)/f_x$
-0.10
-0.08
-0.06
-0.04
-0.02
0.00
0.02
0.04
0.06
0.08
0
1
2
3
4
5
z/a
loading plane
nonhomogeneous medium
homogeneous medium
(e) $\sigma_{yz}(b,a,z)/f_x$
h/a=1
λ=0, λ=0.5
λ=1, λ=1.5
λ=2, λ=2.5
λ=3

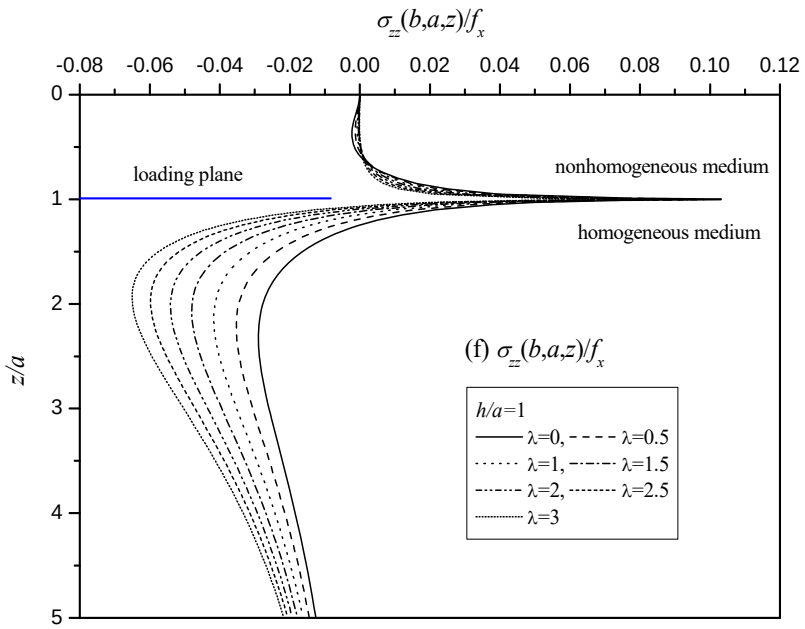

Fig.11 Variation of the stresses at the point (b, a, z) because of f_x located at $h=a$ for different λ

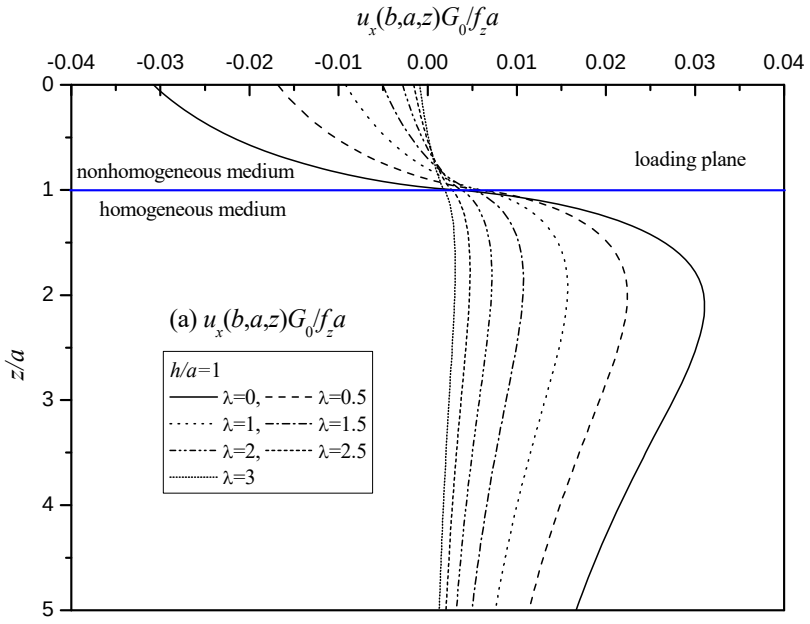

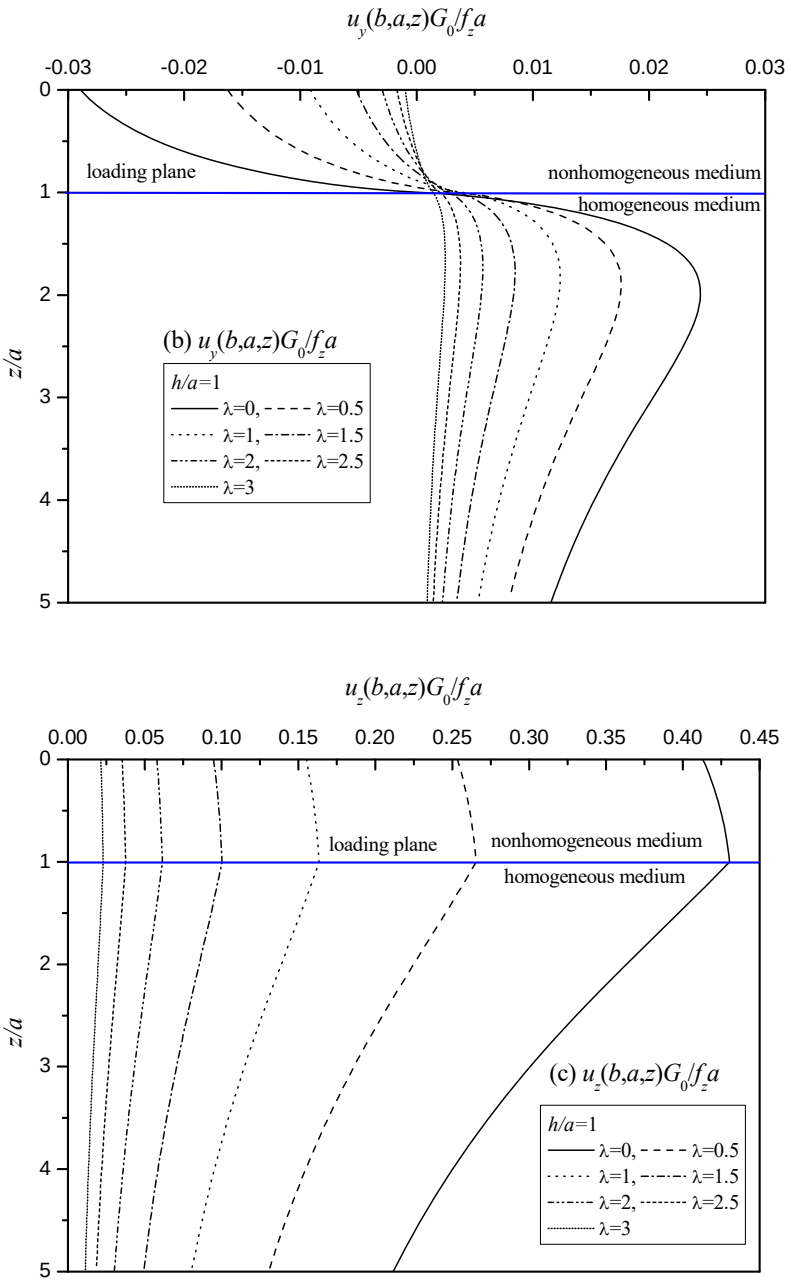

Fig.12 Variation of the displacement at the point (b, a, z) because of f_z located at $h=a$ for different λ

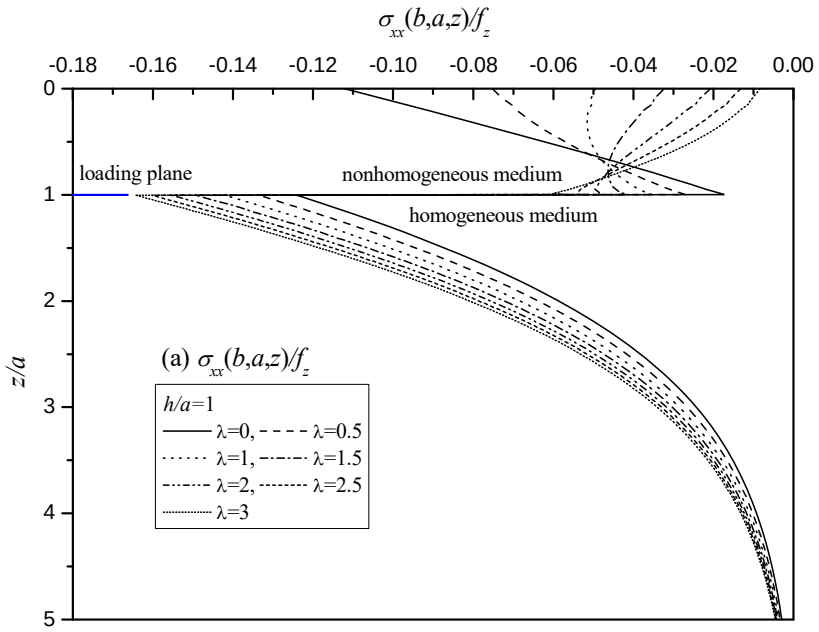
$\sigma_{xx}(b,a,z)/f_z$
-0.18 -0.16 -0.14 -0.12 -0.10 -0.08 -0.06 -0.04 -0.02 0.00
0 1 2 3 4 5
z/a
loading plane
nonhomogeneous medium
homogeneous medium
(a) $\sigma_{xx}(b,a,z)/f_z$
h/a=1
λ=0, λ=0.5
λ=1, λ=1.5
λ=2, λ=2.5
λ=3

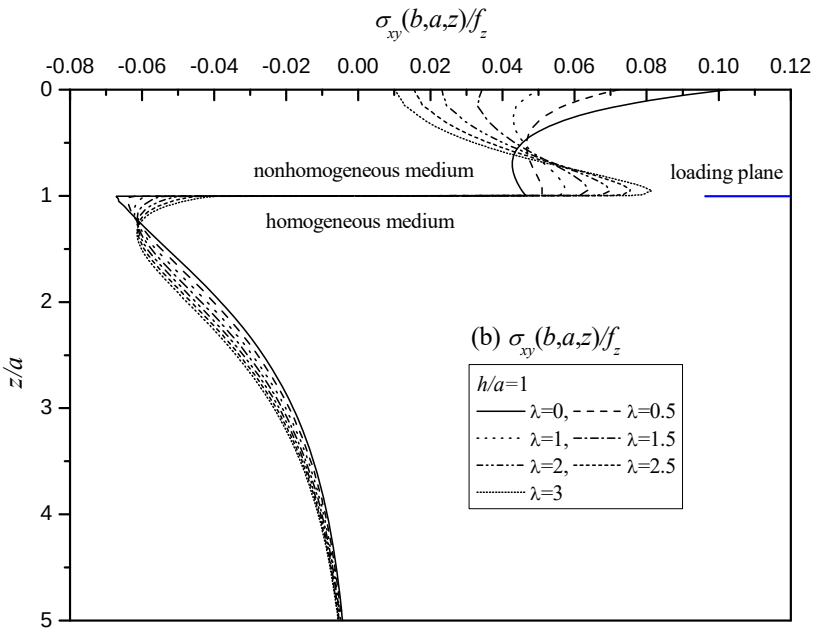
$\sigma_{xy}(b,a,z)/f_z$
-0.08 -0.06 -0.04 -0.02 0.00 0.02 0.04 0.06 0.08 0.10 0.12
0 1 2 3 4 5
z/a
nonhomogeneous medium
loading plane
homogeneous medium
(b) $\sigma_{xy}(b,a,z)/f_z$
h/a=1
λ=0, λ=0.5
λ=1, λ=1.5
λ=2, λ=2.5
λ=3

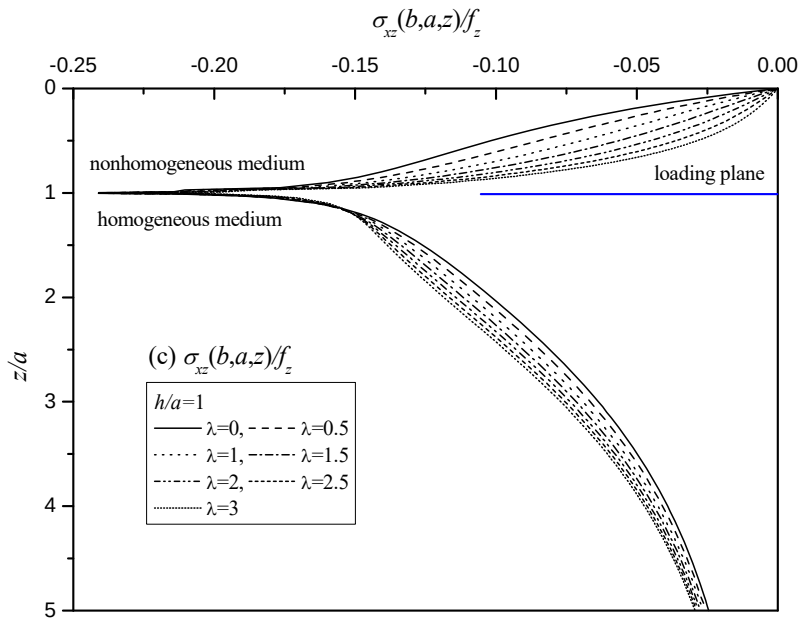
$\sigma_{xz}(b,a,z)/f_z$
-0.25
-0.20
-0.15
-0.10
-0.05
0.00
0
1
2
3
4
5
z/a
nonhomogeneous medium
loading plane
homogeneous medium
(c) $\sigma_{xz}(b,a,z)/f_z$
h/a=1
λ=0, λ=0.5
λ=1, λ=1.5
λ=2, λ=2.5
λ=3

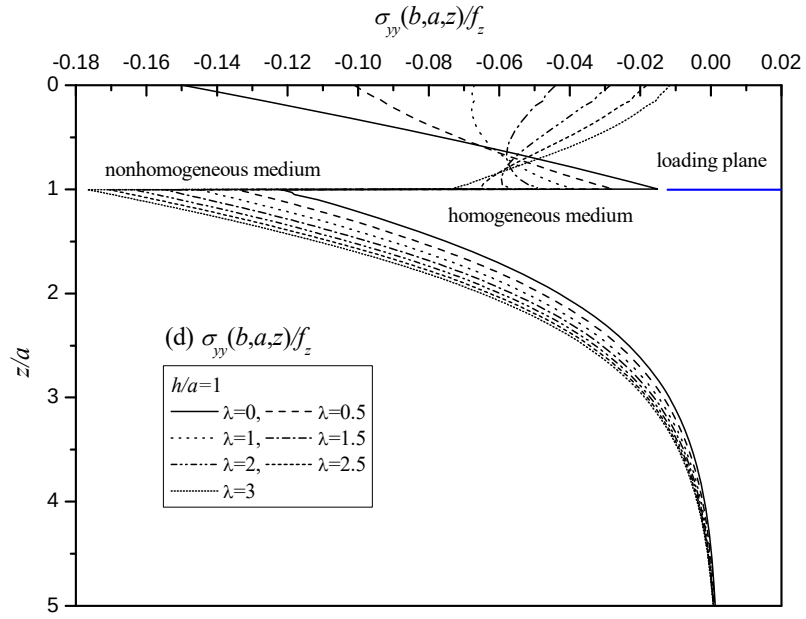
$\sigma_{yy}(b,a,z)/f_z$
-0.18
-0.16
-0.14
-0.12
-0.10
-0.08
-0.06
-0.04
-0.02
0.00
0.02
0
1
2
3
4
5
z/a
nonhomogeneous medium
loading plane
homogeneous medium
(d) $\sigma_{yy}(b,a,z)/f_z$
h/a=1
λ=0, λ=0.5
λ=1, λ=1.5
λ=2, λ=2.5
λ=3

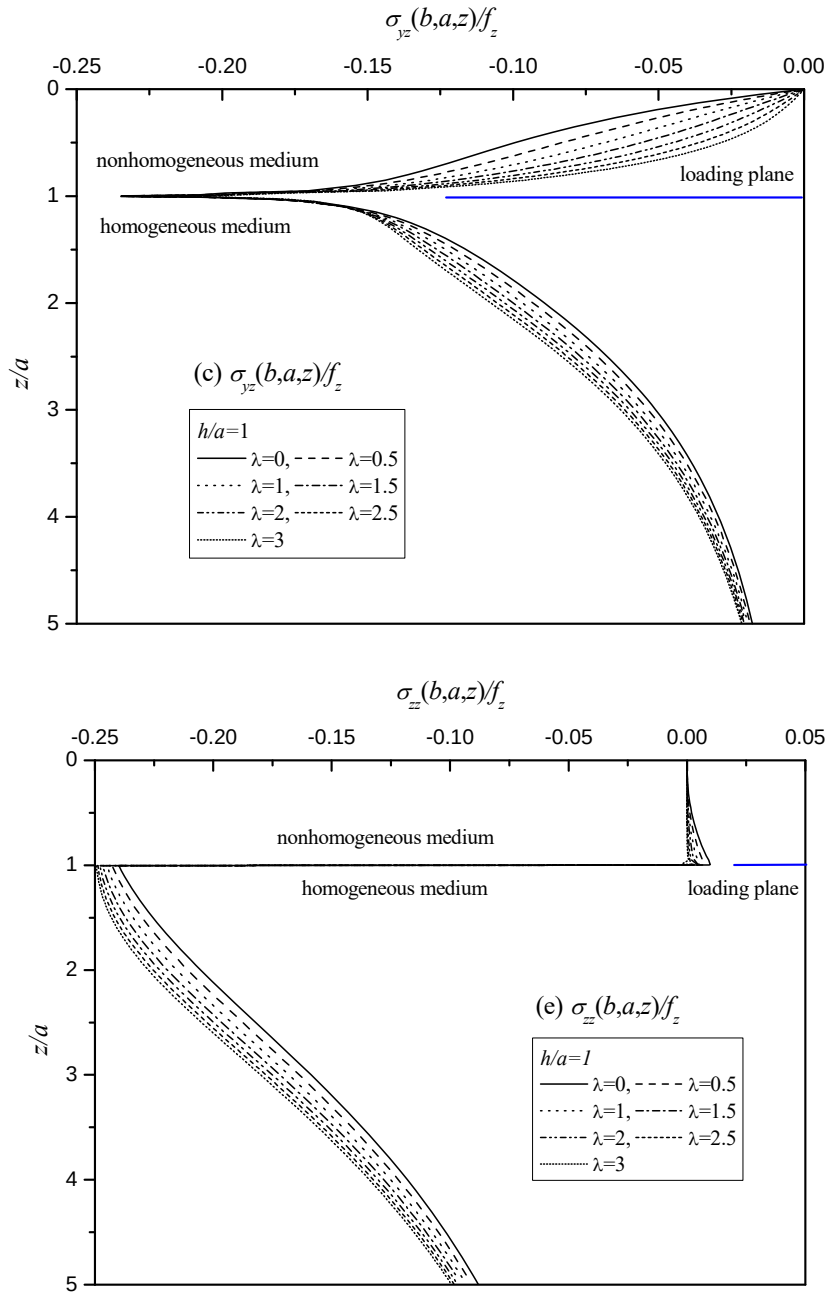

Fig.13 Variation of the stresses at the point (b, a, z) because of f_z located at $h=a$ for different λ

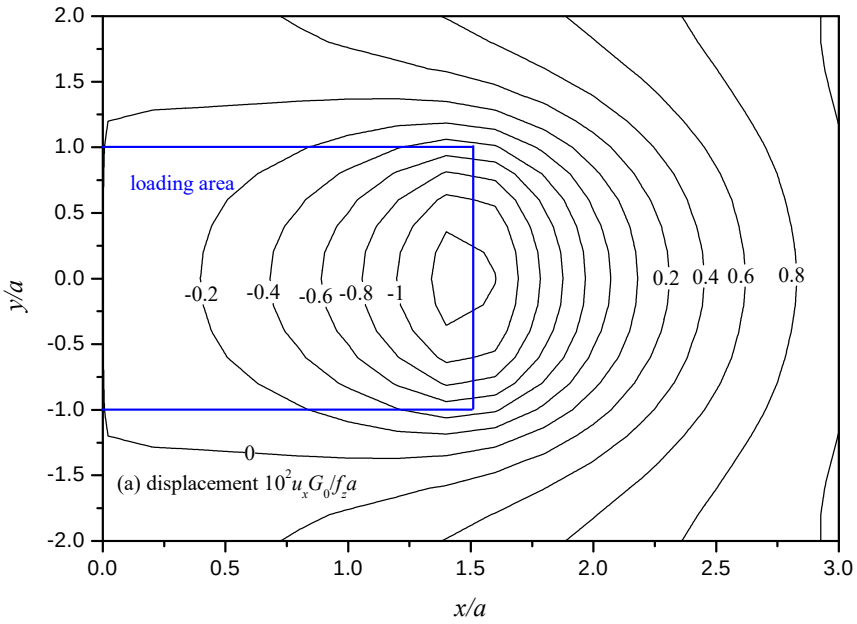
loading area
-0.2
-0.4
-0.6
-0.8
-1
0.2
0.4
0.6
0.8
0
(a) displacement $10^2 u_x G_0/f_z a$
y/a
x/a

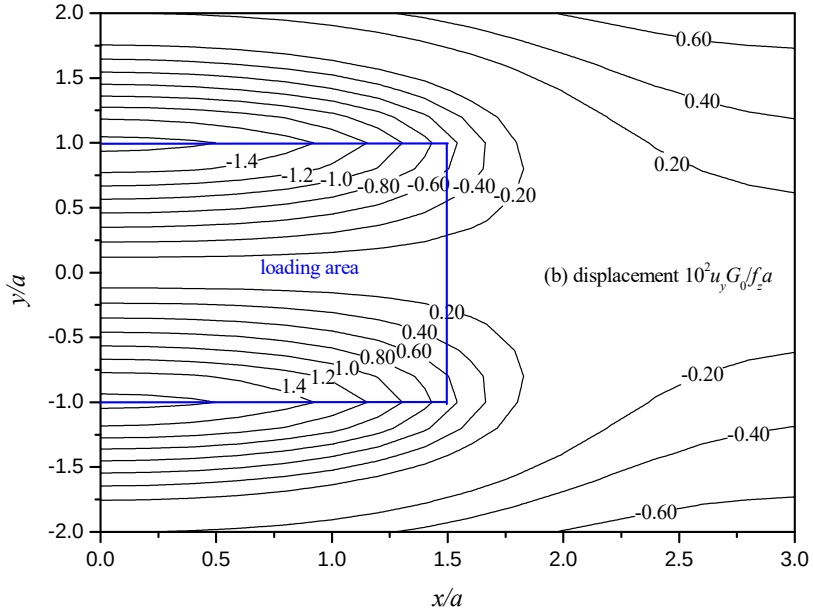
0.60
0.40
0.20
-1.4
-1.2
-1.0
-0.80
-0.60
-0.40
-0.20
loading area
(b) displacement $10^2 u_y G_0/f_z a$
0.20
0.40
0.60
0.80
1.0
1.2
1.4
-0.20
-0.40
-0.60
y/a
x/a

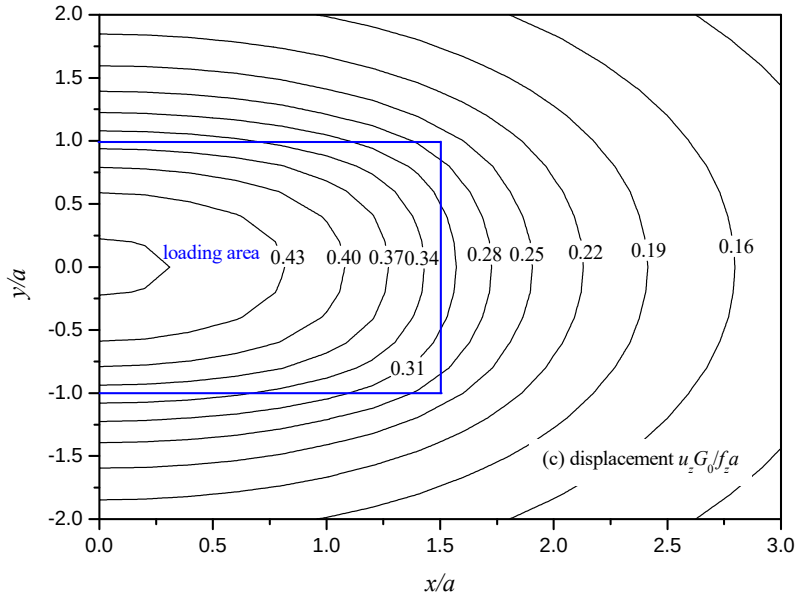

Fig.14 The contours of the three displacements because of f_z located at $h=a$ for $\lambda=0.5$ and $z=0.75a$

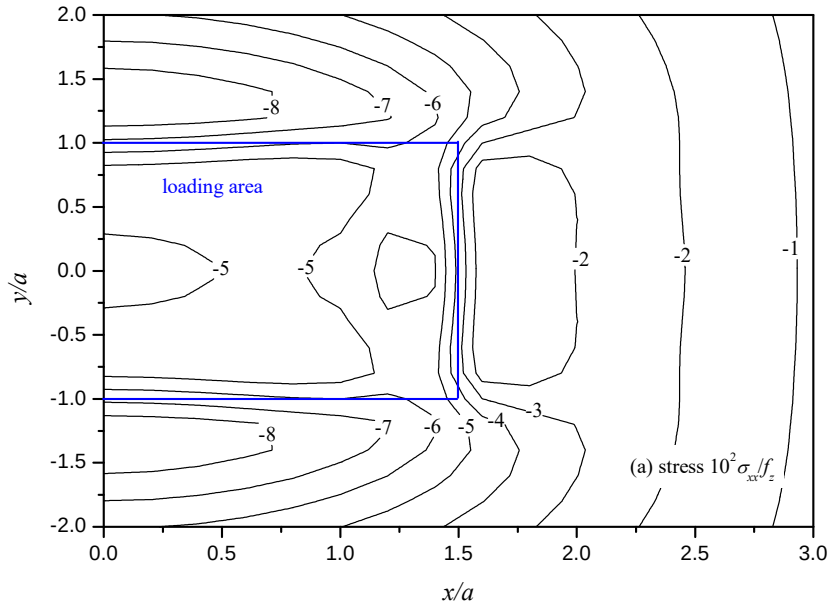

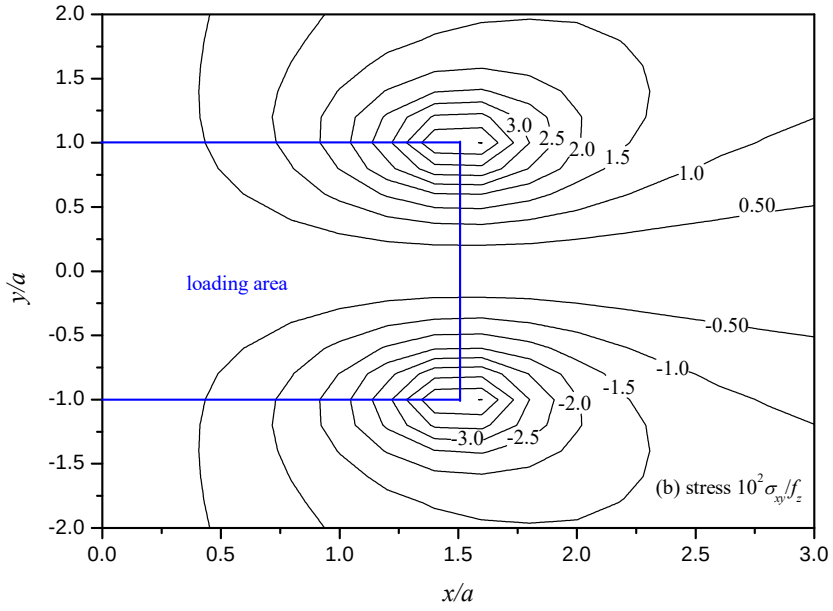
loading area
3.0
2.5
2.0
1.5
1.0
0.50
-0.50
-1.0
-1.5
-2.0
-2.5
-3.0
(b) stress $10^2\sigma_{xy}/f_z$
y/a
x/a

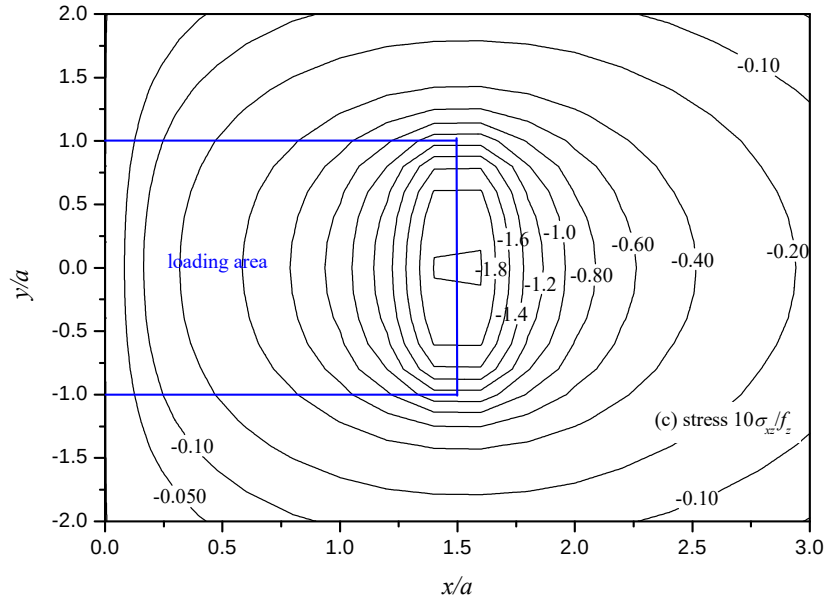
loading area
-0.10
-0.20
-0.40
-0.60
-0.80
-1.0
-1.2
-1.4
-1.6
-1.8
-0.050
(c) stress $10\sigma_{xz}/f_z$
y/a
x/a

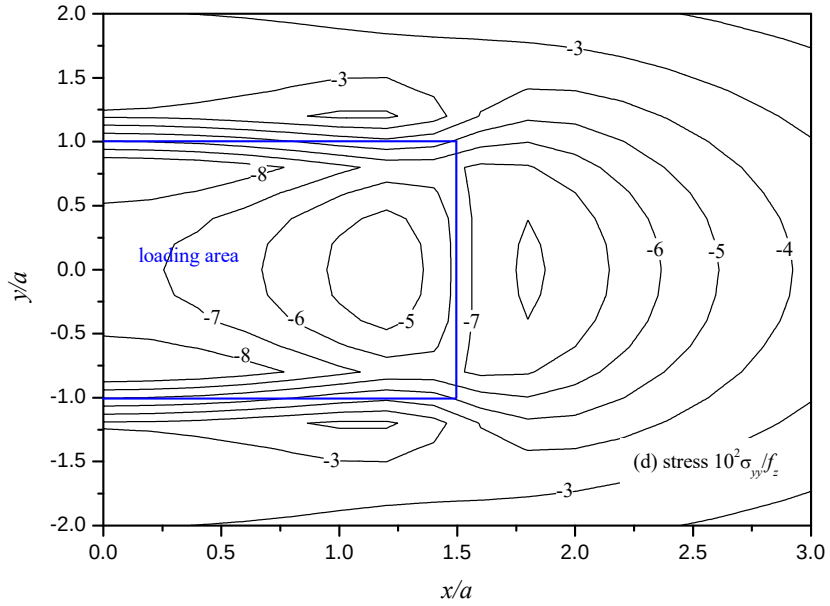
loading area
-3
-8
-7
-6
-5
-4
(d) stress $10^2\sigma_{yy}/f_z$
y/a
x/a

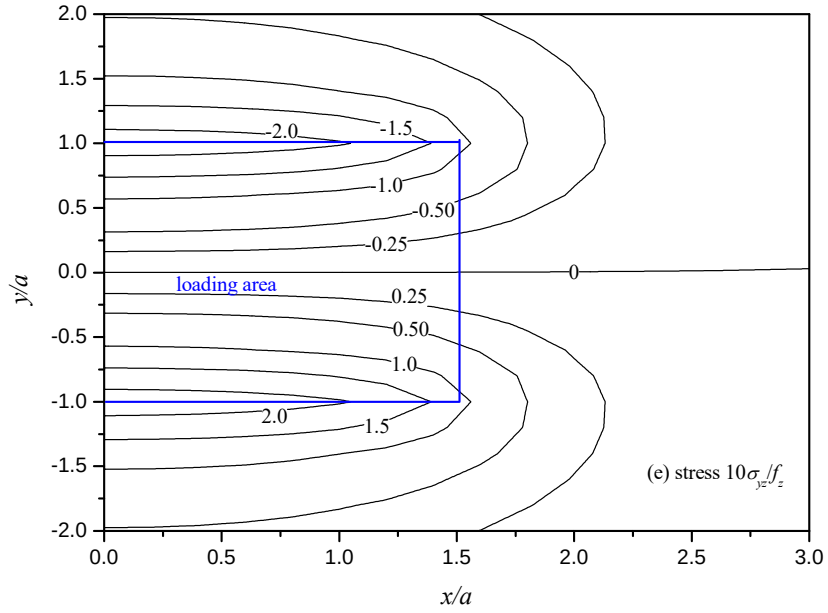
loading area
-2.0
-1.5
-1.0
-0.50
-0.25
0
0.25
0.50
1.0
1.5
2.0
(e) stress $10\sigma_{yz}/f_z$
y/a
x/a

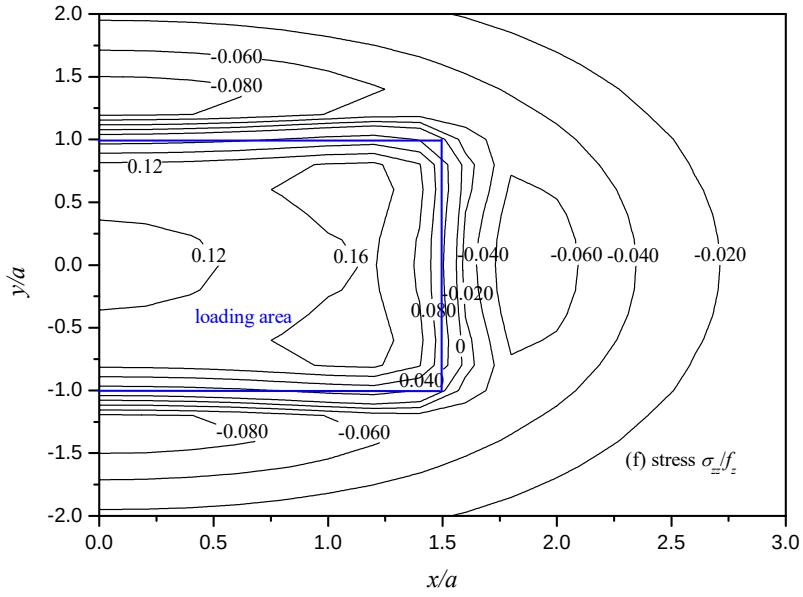

Fig. 15 The contours of the six stress components because of f_z located at $h=a$ for $\lambda=0.5$ and $z=0.75a$

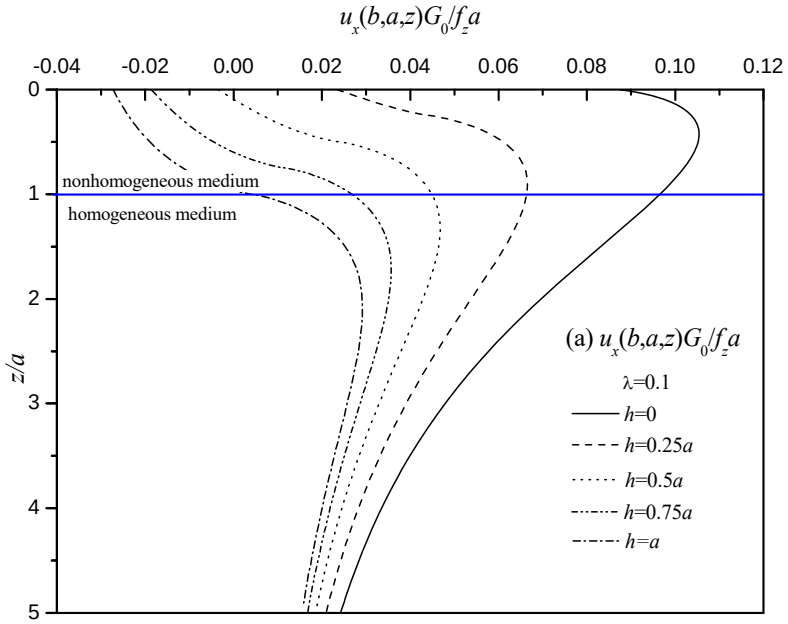

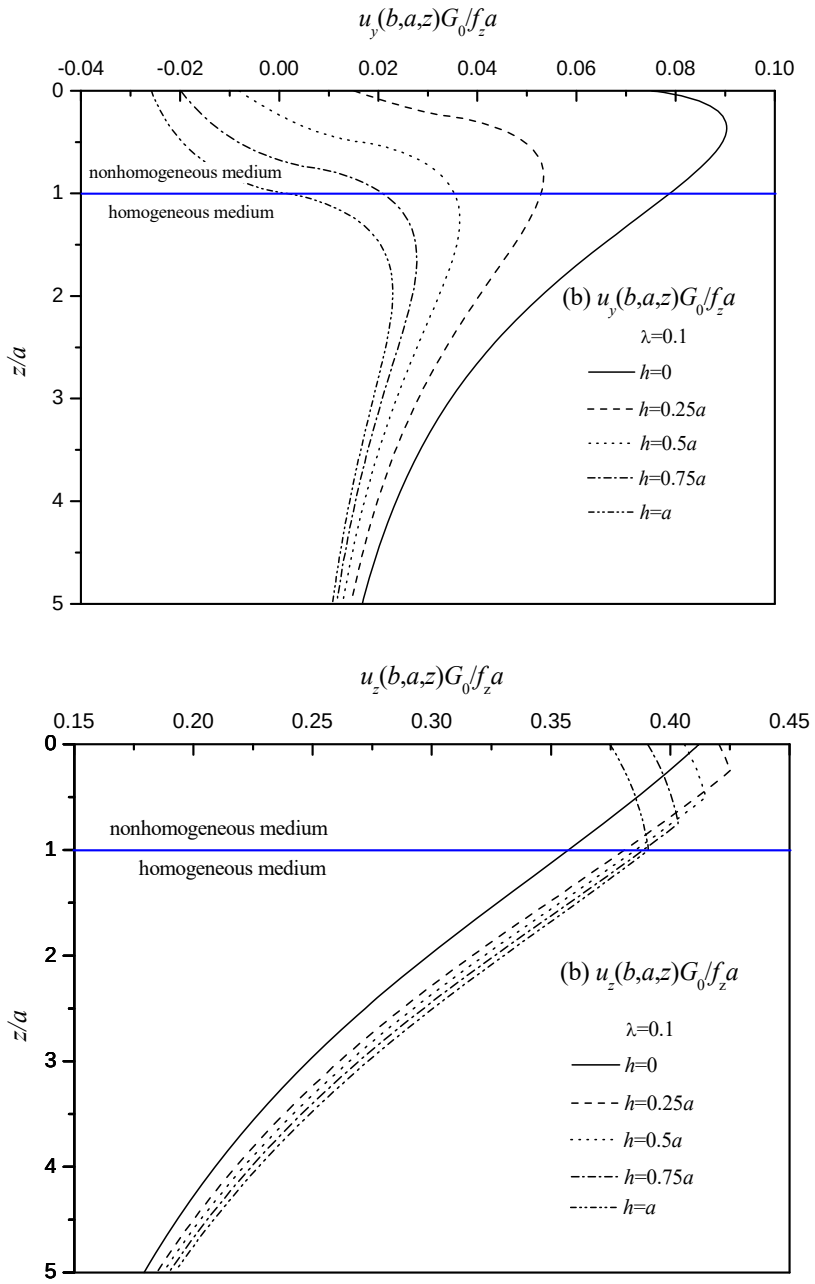

Fig. 16 Variation of three displacements at the point (b, a, z) because of f_z for different h (λ=0.1)

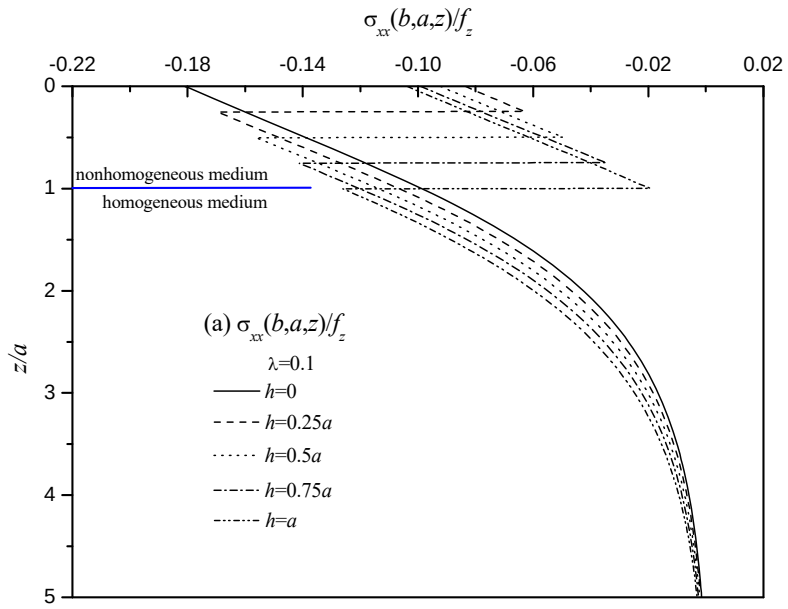
σxx(b,a,z)/fz
-0.22
-0.18
-0.14
-0.10
-0.06
-0.02
0.02
0
1
2
3
4
5
z/a
nonhomogeneous medium
homogeneous medium
(a) σxx(b,a,z)/fz
λ=0.1
h=0
h=0.25a
h=0.5a
h=0.75a
h=a

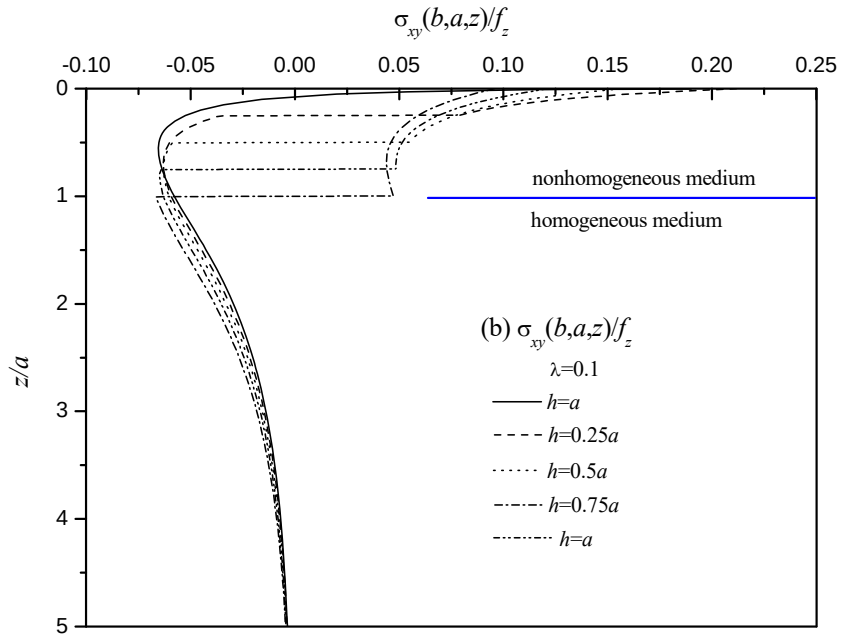
σxy(b,a,z)/fz
-0.10
-0.05
0.00
0.05
0.10
0.15
0.20
0.25
0
1
2
3
4
5
z/a
nonhomogeneous medium
homogeneous medium
(b) σxy(b,a,z)/fz
λ=0.1
h=a
h=0.25a
h=0.5a
h=0.75a
h=a

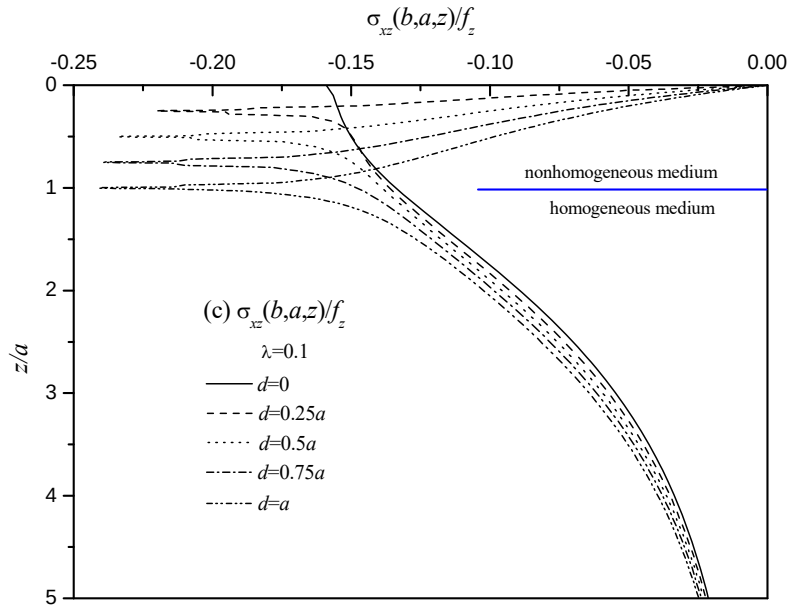
σxz(b,a,z)/fz
-0.25
-0.20
-0.15
-0.10
-0.05
0.00
0
1
2
3
4
5
z/a
nonhomogeneous medium
homogeneous medium
(c) σxz(b,a,z)/fz
λ=0.1
d=0
d=0.25a
d=0.5a
d=0.75a
d=a

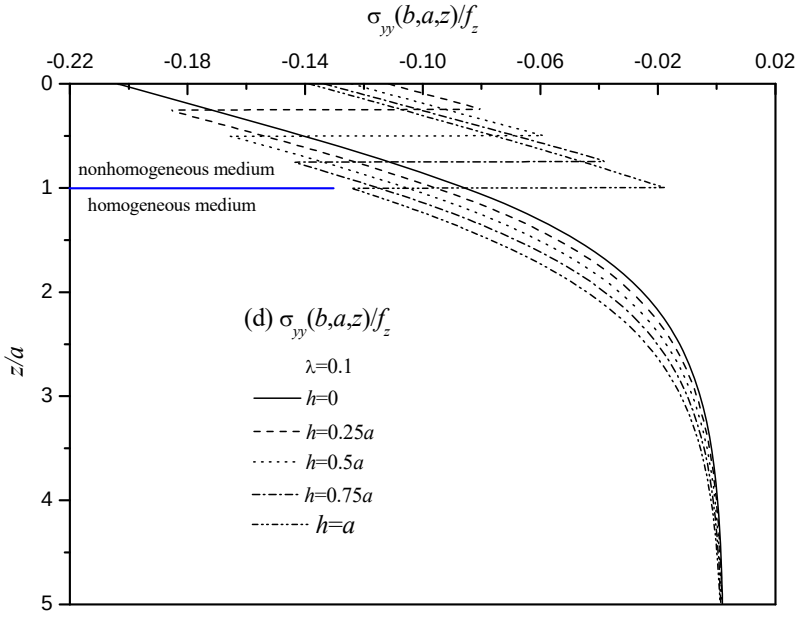
σyy(b,a,z)/fz
-0.22
-0.18
-0.14
-0.10
-0.06
-0.02
0.02
0
1
2
3
4
5
z/a
nonhomogeneous medium
homogeneous medium
(d) σyy(b,a,z)/fz
λ=0.1
h=0
h=0.25a
h=0.5a
h=0.75a
h=a

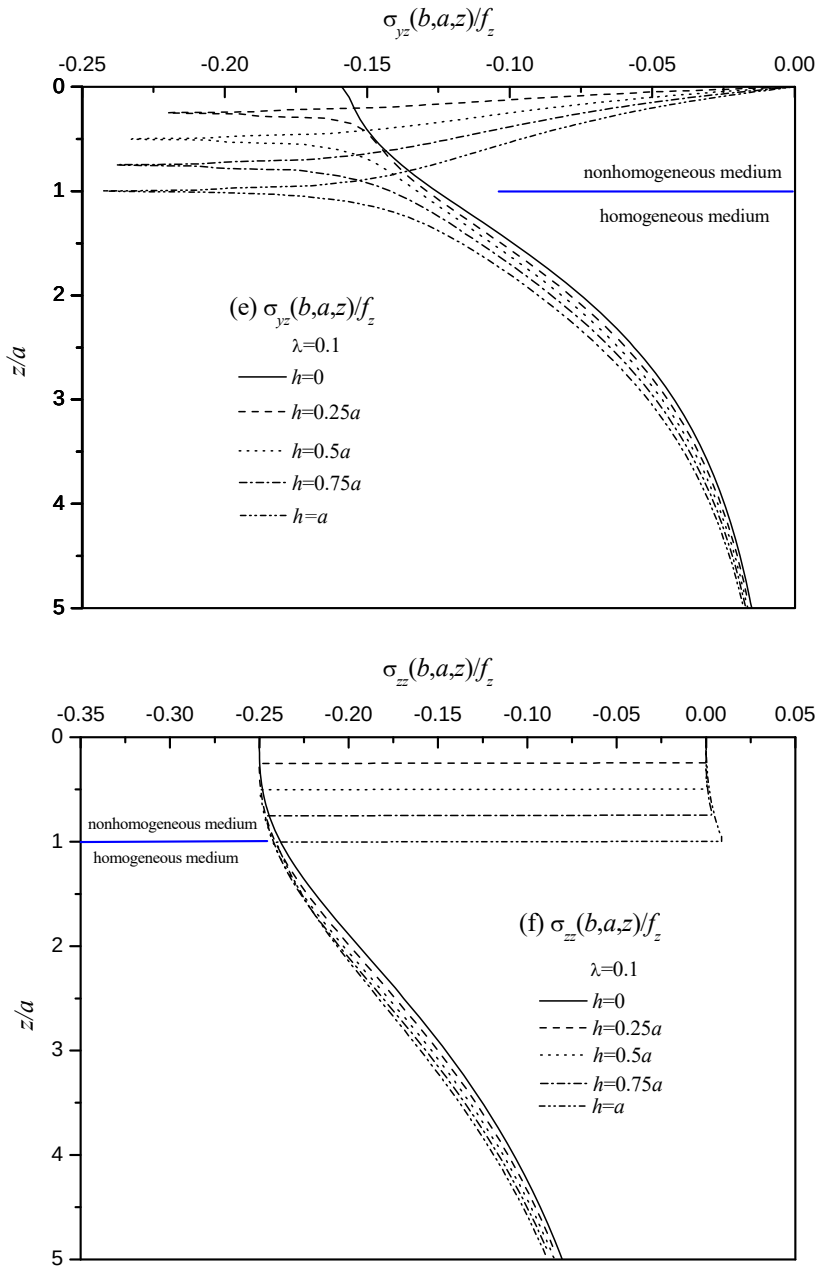

Fig. 17 Variations of the six stresses at the point (b, a, z) because of f_z for different h (λ=0.1)

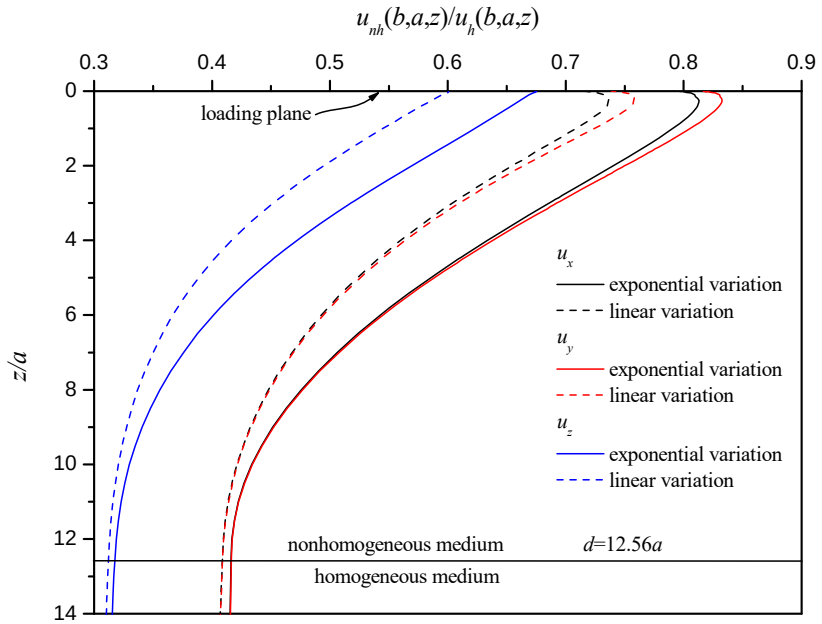

Fig. 18 Ratio of three displacements at the point (b, a, z) because of f_z in a non-homogeneous medium to a homogeneous medium

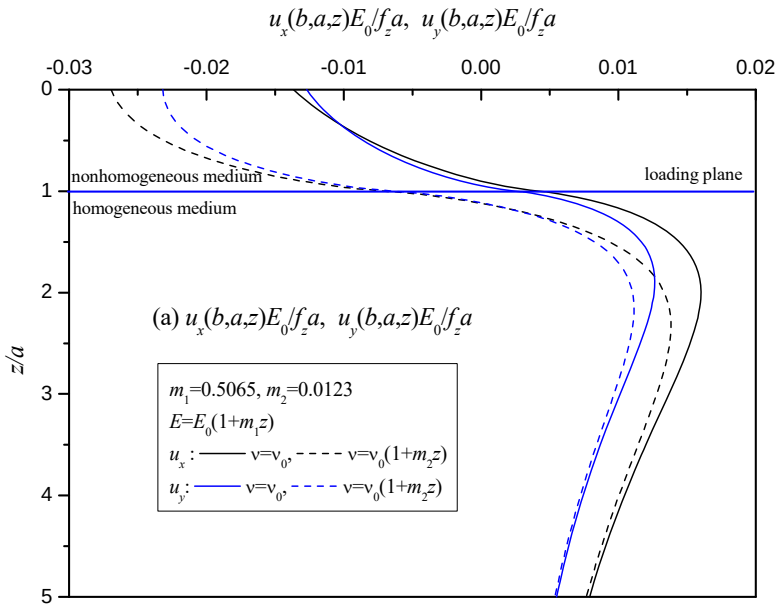

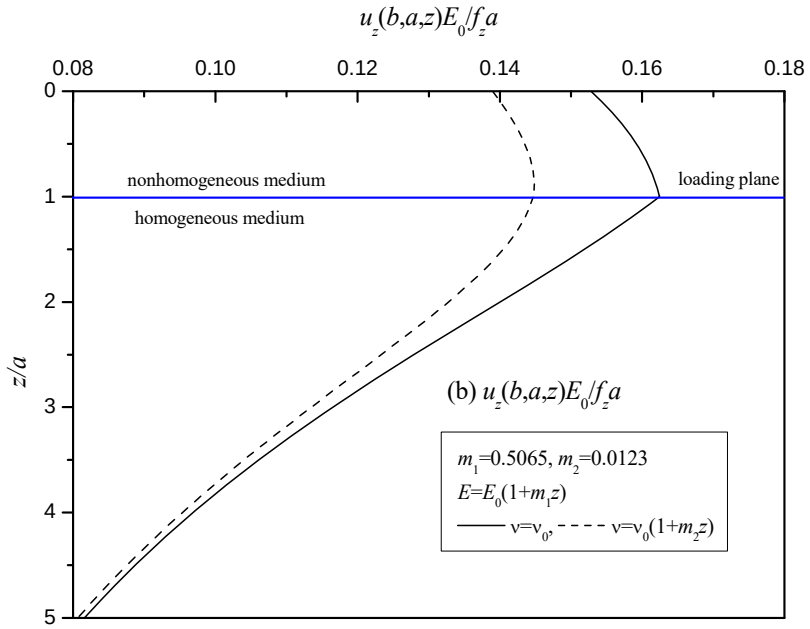

Fig. 19 Variations of the displacements at the point (b, a, z) because of f_z for different v

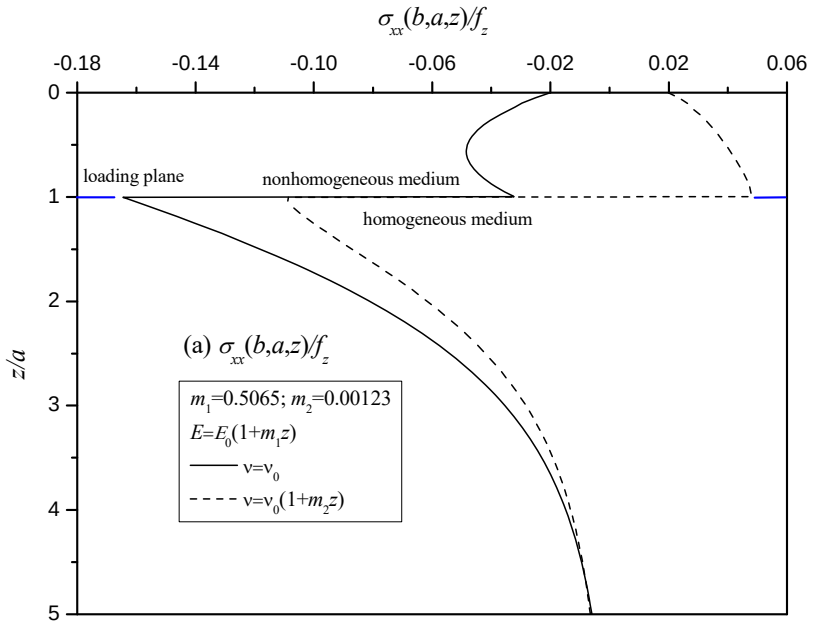

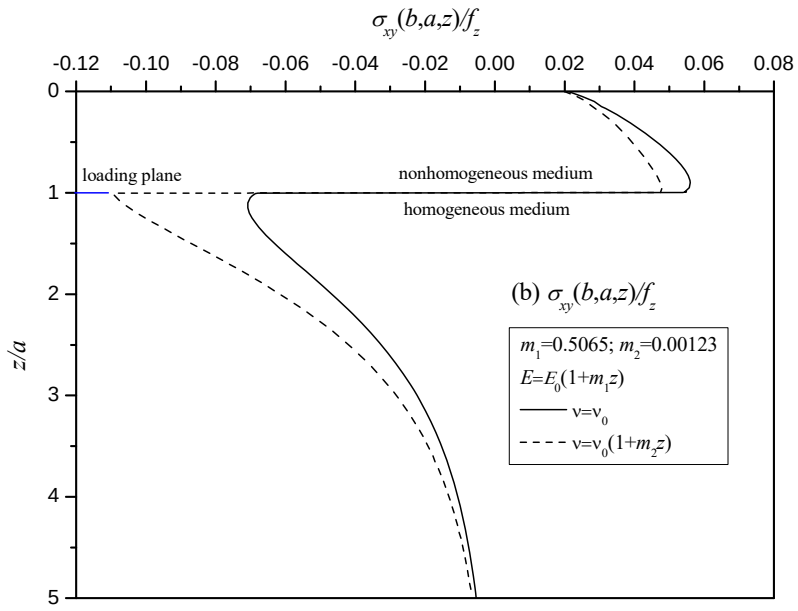
$\sigma_{xy}(b,a,z)/f_z$
-0.12 -0.10 -0.08 -0.06 -0.04 -0.02 0.00 0.02 0.04 0.06 0.08
0
1
2
3
4
5
z/a
loading plane
nonhomogeneous medium
homogeneous medium
(b) $\sigma_{xy}(b,a,z)/f_z$
m_1=0.5065; m_2=0.00123
$E=E_0(1+m_1z)$
ν=ν$_0$
ν=ν$_0$(1+m_2z)

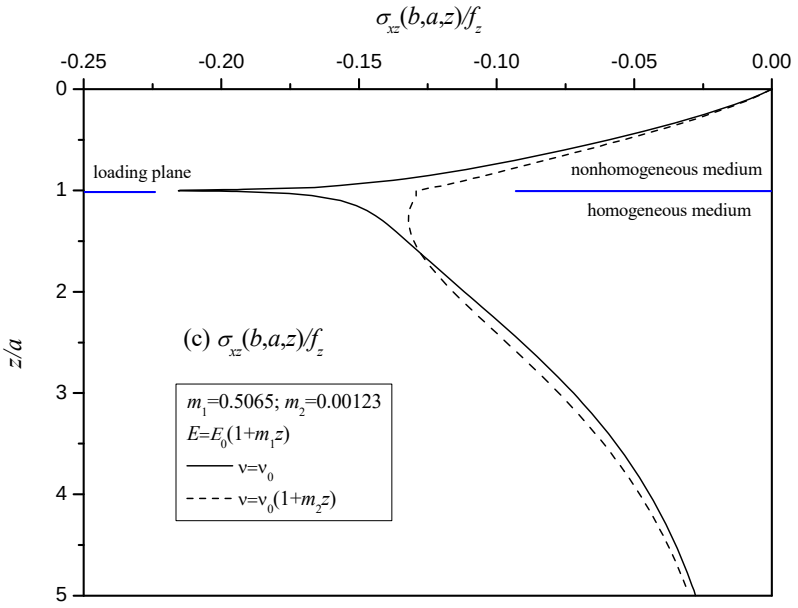
$\sigma_{xz}(b,a,z)/f_z$
-0.25 -0.20 -0.15 -0.10 -0.05 0.00
0
1
2
3
4
5
z/a
loading plane
nonhomogeneous medium
homogeneous medium
(c) $\sigma_{xz}(b,a,z)/f_z$
m_1=0.5065; m_2=0.00123
$E=E_0(1+m_1z)$
ν=ν$_0$
ν=ν$_0$(1+m_2z)

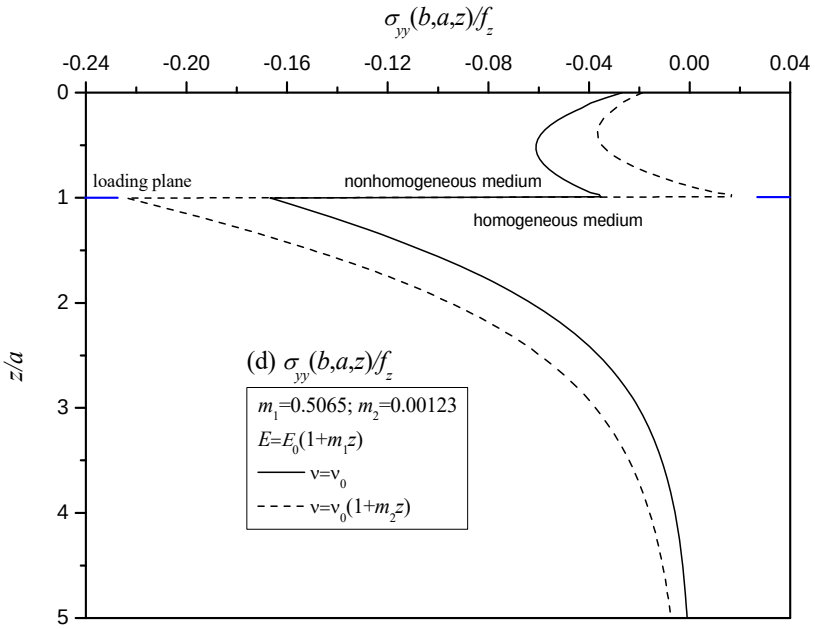
$\sigma_{yy}(b,a,z)/f_z$
-0.24
-0.20
-0.16
-0.12
-0.08
-0.04
0.00
0.04
0
1
2
3
4
5
z/a
loading plane
nonhomogeneous medium
homogeneous medium
(d) $\sigma_{yy}(b,a,z)/f_z$
m_1=0.5065; m_2=0.00123
$E=E_0(1+m_1z)$
ν=ν$_0$
ν=ν$_0$(1+m_2z)

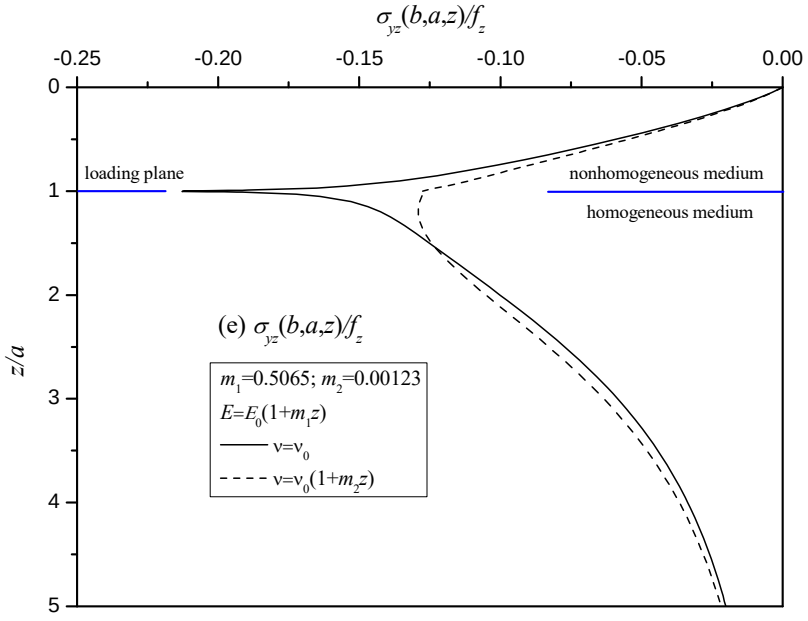
$\sigma_{yz}(b,a,z)/f_z$
-0.25
-0.20
-0.15
-0.10
-0.05
0.00
0
1
2
3
4
5
z/a
loading plane
nonhomogeneous medium
homogeneous medium
(e) $\sigma_{yz}(b,a,z)/f_z$
m_1=0.5065; m_2=0.00123
$E=E_0(1+m_1z)$
ν=ν$_0$
ν=ν$_0$(1+m_2z)

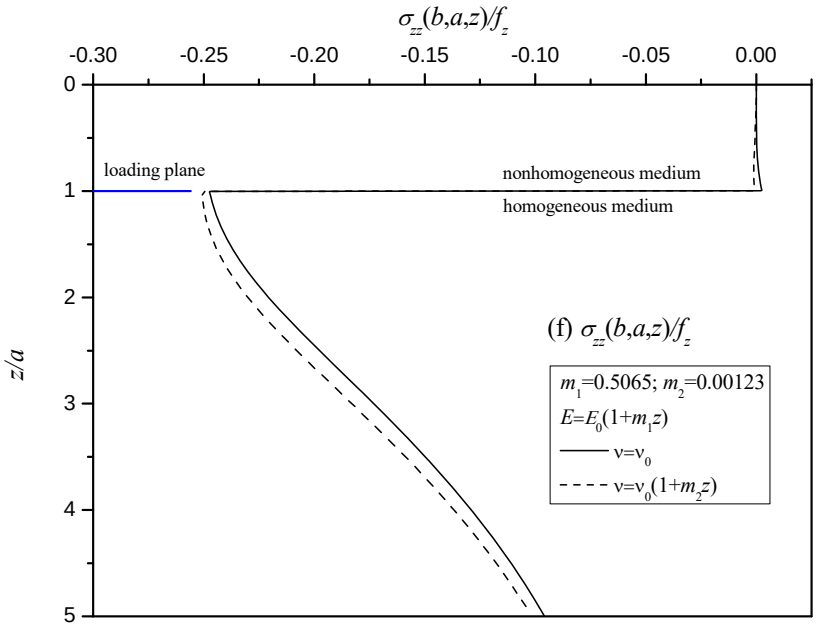

Fig. 20 Variations of the stresses at the point (b, a, z) because of f_z for different v

Table 1 The minimum M value for the relative error less than 1%

z/a	0.03	0.05	0.1	0.2	0.3	0.4	0.5
u_z	5	3	1	1	0	0	0
σ_{zz}	15	9	3	1	0	0	0

Table 2 Subroutine CALSTRESDISPL-shared memory version

```
subroutine CALSTRESDISPL
    …
    internal points: do i=1,NPIN
    xp(:)=xyzin(:,i)
    !$OMP PARALLEL DEFAULT(SHARED)
    !$OMP DO PRIVATE(j,xe,ie,k)
      elements: do j=1,NE
      do ie=1,8
        k=nep(ie,j);  xe(:,ie)=xyz(:,k)
      enddo
!     compute the coefficients: cofu and cofs
      call iks(xp,xe,nep,cofu, cofs,…)
      do ie=1,8
        do k=1,3
!         compute the stresses at internal point i
          strs(:,:,i)= strs(:,:,i)+cofs(:,:,k,ie,i)*te(k,ie,i)
!         compute the displacement at internal point i
          displ(:,i)= displ(:,i)+cofu(:,k,ie,i)*te(k,ie,i)
        enddo
      enddo
      enddo elements
    !$OMP END DO
    !$OMP END PARALLEL
    enddo internal points
    …
end subroutine CALSTRESDISPL
```

Table 3 Results of vertical displacement $u_z(0,0,0)G_0 / f_z a$ for different λ by the present study and Katebi and Selvadurai (2013)

No. of a layered elastic halfspace	λ=0.5	λ=1	λ=2	λ=3
10	0.216108	0.131272	0.0477420	0.0171478
15	0.216245	0.131386	0.0477666	0.0171379
20	0.216314	0.131449	0.0477834	0.0171360
25	0.216357	0.131487	0.0477943	0.0171357
30	0.216386	0.131511	0.0478019	0.0171358
35	0.216408	0.131528	0.0478072	0.0171360
40	0.216423	0.131539	0.0478115	0.0171362
50	0.216444	0.131562	0.0478193	0.0171372
60	0.216456	0.131577	0.0478235	0.0171377
80	0.216478	0.131588	0.0478277	0.0171381
100	0.216488	0.131583	0.0478289	0.0171380
Katebi & Selvadurai	0.215587	0.131306	0.048468	0.017871

Table 4 Comparison of CPU times (s) between serial and parallel computations

Mesh No.	Number of discrete layers	CPU^S for serial computation	CPU^P for parallel computation	CPU^S/ CPU^P
1	50	29	2	14.5
	100	86	6	14.3
2	50	129	8	16.1
	100	358	24	14.9
3	50	516	28	18.4
	100	1410	98	14.4

Computer configuration：HP workstation SC001, Xeon CPU 1.7GHz, 16GB RAM.